Polyhedron 30 (2011) 1830–1841

Contents lists available at ScienceDirect

Polyhedron

journal homepage: www.elsevier.com/locate/poly

Syntheses and properties of complexes with bis(2,2′-bipyridyl)ruthenium(II) moieties coordinated to 4,4′:2′,2″:4″,4‴-quaterpyridinium ligands

Benjamin J. Coe *, Elizabeth C. Harper, Madeleine Helliwell, Yien T. Ta

School of Chemistry, University of Manchester, Oxford Road, Manchester M13 9PL, UK

ARTICLE INFO

Article history:
Received 21 March 2011
Accepted 12 April 2011
Available online 23 April 2011

Keywords:
Ruthenium complexes
Polypyridyl ligands

ABSTRACT

Eleven new complexes of the form *cis*-$[Ru^{II}(bpy)_2(L^A)]^{4+}$ (bpy = 2,2′-bipyridyl; L^A = a pyridinium-substituted bpy derivative) have been prepared and isolated as their PF_6^- salts. Characterisation involved various techniques including ^1H NMR spectroscopy and MALDI mass spectrometry. The UV–Vis spectra show intense intraligand $\pi \rightarrow \pi^*$ absorptions and metal-to-ligand charge-transfer (MLCT) bands with two distinct maxima in the visible region. Small shifts in the MLCT bands correlate with the electron-withdrawing strength of the ligand L^A. Cyclic voltammograms show quasi-reversible or reversible $Ru^{III/II}$ oxidation waves, and two or more ligand-based reductions with varying degrees of reversibility. The variations in the redox potentials correlate with changes in the structure of L^A, and also with the MLCT energies. Differential pulse voltammetry allows the first reduction process for two of the complex salts to be resolved into two peaks. Single-crystal X-ray structures have been solved for three of the new complex salts and also for a pro-ligand salt. Two carboxylate-functionalised compounds have been tested as photosensitizers on TiO_2-coated electrodes, but show only negligible efficiencies, in accord with expectations.

1. Introduction

Amongst the transition metals, ruthenium displays an especially diverse coordination and organometallic chemistry, including a vast array of stable complexes with every conceivable type of ligand [1]. An ideal combination of relatively high stability and synthetic accessibility has underpinned the development of this field. Of the range of formal oxidation states available to this metal, the +2 and +3 ions are especially widely studied. In addition to pure chemical interest and fundamental scientific value, Ru complexes have attracted attention for practical applications in a number of important areas including catalysis [2], medicine [3], and technologies that exploit the photophysical/chemical properties of Ru^{II}-based chromophores [4]. The latter encompass fields such as organic light-emitting diodes [5] and dye-sensitized solar cells [6]. Such applications based on photoactivity involve complexes of chelating polypyridyl ligands, of which $[Ru^{II}(bpy)_3]^{2+}$ (RuTB; bpy = 2,2′-bipyridyl) is the prototype [7]. The rich electronic absorption, emission and electron-transfer properties of RuTB and related complexes arise from the presence of low energy metal-to-ligand charge-transfer (MLCT) excited states. The ability to tune the properties of such states *via* modifications in ligand structure is now a very well developed area of coordination chemistry [4].

Another area in which Ru complexes have featured extensively is that of nonlinear optical (NLO) chromophores and materials [8]. As part of our ongoing studies in this field, we have investigated a number of complexes of 4,4′:2′,2″:4″,4‴-quaterpyridinium ligands. These include V-shaped dipolar structures with electron-rich *cis*-$\{Ru^{II}(NH_3)_4\}^{2+}$ centres [9], as well as octupolar tris-chelates that are derivatives of RuTB [10,11]. These complexes show especially intense, broad MLCT absorption profiles, which in the case of the tris-chelates feature two well-resolved bands. The MLCT transitions are associated with relatively large second- and third-order NLO responses [9–11]. The present study involves a series of new complexes that can be viewed as hybrids of those reported previously, in that they contain a RuTB core but with only one quaterpyridinium ligand. The optical spectroscopic and electrochemical properties of the new species are compared with those of the existing compounds, and several X-ray crystallographic studies are presented.

2. Experimental

2.1. Materials, procedures and physical measurements

All reactions were performed under an Ar atmosphere. The compounds *cis*-$Ru^{II}Cl_2(bpy)_2{\cdot}2H_2O$ [12], 4,4′-di[(*E*)-2-(*N*-methyl-4-pyri-

* Corresponding author. Tel.: +44 (0)161 275 4601; fax: +44 (0)161 275 4598.
E-mail addresses: B.Coe@man.ac.uk, b.coe@manchester.ac.uk (B.J. Coe).
URL: http://www.chemistry.manchester.ac.uk/aboutus/staff/show.html?ea=Benjamin.Coe (B.J. Coe).

0277-5387/$ - see front matter © 2011 Elsevier Ltd. All rights reserved.
doi:10.1016/j.poly.2011.04.018

dyl)vinyl]-2,2′-bipyridyl iodide ([Me_2bbpe^{2+}]I_2) [13], 4,4′-di[(*E*)-2-(*N*-phenyl-4-pyridyl)vinyl]-2,2′-bipyridyl chloride ([Ph_2bbpe^{2+}]Cl_2) [13], and 4,4′-di{(*E*)-2-[*N*-(2,4-dinitrophenyl)-4-pyridyl]vinyl}-2,2′-bipyridyl chloride ([$(2,4\text{-}DNPh)_2bbpe^{2+}$]$Cl_2$) [13], were prepared according to published procedures. The compounds *N*″,*N*‴-diphenyl-4,4′:2′,2″:4″,4‴-quaterpyridinium chloride ([Ph_2qpy^{2+}]Cl_2) [9], *N*″,*N*‴-di(4-acetylphenyl)-4,4′:2′,2″:4″,4‴-quaterpyridinium chloride ([$(4\text{-}AcPh)_2qpy^{2+}$]$Cl_2$) [9], *N*″,*N*‴-di(2-pyrimidyl)-4,4′:2′,2″:4″,4‴-quaterpyridinium chloride ([$(2\text{-}Pym)_2qpy^{2+}$]Cl_2) [9], *N*″,*N*‴-di(2,4-dinitrophenyl)-4,4′:2′,2″:4″,4‴-quaterpyridinium chloride ([$(2,4\text{-}DNPh)_2qpy^{2+}$]$Cl_2$) [10] and *N*″,*N*‴-di(3,5-bismethoxycarbonylphenyl)-4,4′:2′,2″:4″,4‴-quaterpyridinium chloride ([$(3,5\text{-}MC_2Ph)_2qpy^{2+}$]$Cl_2$) [10] were prepared by modifying published methods in which these chloride salts were treated as intermediates, with no analytical data being obtained. All other reagents were obtained commercially and used as supplied. Products were dried overnight in a vacuum dessicator ($CaSO_4$) prior to characterisation.

^{1}H NMR spectra were recorded on a Bruker AV-400 spectrometer and all shifts are quoted with respect to TMS. The fine splitting of pyridyl or phenyl ring AA′BB′ patterns is ignored and the signals are reported as simple doublets, with *J* values referring to the two most intense peaks. In cases where there is any uncertainty about their assignments, based on splitting patterns and integrals, signals for pyridyl (C_5H_3N or C_5H_4N) ring protons are denoted simply by "py". Elemental analyses were performed by the Microanalytical Laboratory, University of Manchester. IR spectroscopy was performed on solid samples by using an Excalibur BioRad FT-IR spectrometer, and UV–Vis spectra were obtained by using a Shimadzu UV-2401 PC spectrophotometer. Mass spectra were measured by using +electrospray on a Micromass Platform II spectrometer or MALDI on a Micromass Tof Spec 2e with acetonitrile as the solvent. Cyclic and differential pulse voltammetric measurements were carried out with an Ivium CompactStat. An EG&G PAR K0264 single-compartment microcell was used with a silver/silver chloride reference electrode (3 M NaCl, saturated AgCl) separated by a salt bridge from a glassy carbon disc working electrode and Pt wire auxiliary electrode. Acetonitrile was freshly distilled (from CaH_2) and [NBu^n_4]PF_6, as supplied from Fluka, was used as the supporting electrolyte. Solutions containing *ca.* 10^{-3} M analyte (0.1 M electrolyte) were deaerated by purging with N_2. All $E_{1/2}$ values were calculated from $(E_{pa} + E_{pc})/2$ at a scan rate of 200 mV s^{-1}.

2.2. Syntheses

2.2.1. 4,4′:2′,2″:4″,4‴-Quaterpyridyl, qpy

A mixture of 4,4′-bipyridyl (10.0 g, 64.0 mmol) and 10% Pd on charcoal (2.00 g) was heated at *ca.* 250 °C for 48 h and then cooled to room temperature. Aqueous HCl (2 M, 250 mL) was added, and the black suspension was filtered. Aqueous NaOH (8 M, 75 mL) was added dropwise to the stirred brown filtrate to afford a grey precipitate which was filtered off, washed with water and dried. Purification was achieved by using a silica gel column, eluting with 95:5, followed by 90:10 dichloromethane/methanol after removal of unreacted starting material. The product was obtained as a cream-coloured solid. Yield: 1.86 g (18%). δ_H (400 MHz, $CDCl_3$) 8.83 (2H, dd, *J* = 5.0, 0.8 Hz, C_5H_3N), 8.79–8.77 (6H, C_5H_3N + C_5H_4N), 7.68 (4H, d, *J* = 6.0 Hz, C_5H_4N), 7.61 (2H, dd, *J* = 5.0, 1.8 Hz, C_5H_3N). *Anal.* Calc. (%) for $C_{20}H_{14}N_4{\cdot}0.5H_2O$: C, 75.22; H, 4.73; N, 17.54. Found: C, 75.49; H, 4.42; N, 17.44%.

2.2.2. *N*″,*N*‴-Dimethyl-4,4′:2′,2″:4″,4‴-quaterpyridinium chloride, [Me_2qpy^{2+}]Cl_2

A solution of qpy·0.5H_2O (500 mg, 1.57 mmol) and methyl iodide (2 mL) in acetone (50 mL) was heated at reflux for 4 h. The solution was cooled and a yellow precipitate was filtered off and washed with acetone (50 mL) followed by chloroform (5 × 10 mL). The crude yellow solid, [Me_2qpy^{2+}]I_2, was stirred in warm ethanol (250 mL), then filtered off. The solid was dissolved in water (200 mL) and addition of aqueous NH_4PF_6 afforded a cream-coloured precipitate, [Me_2qpy^{2+}][PF_6]$_2$, which was filtered off, washed with water and dried. The solid was dissolved in acetone (300 mL), the solution filtered, and [NBu^n_4]Cl in acetone was added to the filtrate. The cream-coloured precipitate was filtered off, washed with acetone and dried. Yield: 398 mg (54%). δ_H (400 MHz, CD_3OD) 9.09 (4H, d, *J* = 6.8 Hz, C_5H_4N), 9.04 (2H, dd, *J* = 1.9, 0.6 Hz, C_5H_3N), 9.01 (2H, dd, *J* = 5.0, 0.8 Hz, C_5H_3N), 8.62 (4H, d, *J* = 7.1 Hz, C_5H_4N), 8.07 (2H, dd, *J* = 5.2, 1.9 Hz, C_5H_3N), 4.51 (6H, s, 2Me). *Anal.* Calc. (%) for $C_{22}H_{20}Cl_2N_4{\cdot}3.1H_2O$: C, 56.56; H, 5.65; N, 11.99. Found: C, 56.45; H, 5.27; N, 11.97%. ES-MS: *m*/*z* = 375 ([M−Cl]$^+$), 170 ([M−2Cl]$^{2+}$).

2.2.3. *N*″,*N*‴-Diphenyl-4,4′:2′,2″:4″,4‴-quaterpyridinium chloride, [Ph_2qpy^{2+}]Cl_2

A mixture of qpy·0.5H_2O (500 mg, 1.57 mmol) and 2,4-dinitrochlorobenzene (3.17 g, 15.7 mmol) in ethanol (40 mL) was heated at reflux for 72 h. The solution was allowed to cool and chloroform (30 mL) was added to give a pale brown precipitate, [$(2,4\text{-}DNPh)_2qpy^{2+}$]$Cl_2$, which was filtered off and washed with diethyl ether. The solid was dissolved in DMSO (30 mL) and aniline (1.5 mL) was added. The resulting solution was stirred at 70 °C for 3 h, cooled and then filtered. Acetone (100 mL) was added and a peach-coloured precipitate, [Ph_2qpy^{2+}]Cl_2, was filtered off. The solid was dissolved in water (100 mL) before addition of aqueous NH_4PF_6 to give a beige precipitate, [Ph_2qpy^{2+}][PF_6]$_2$, which was filtered off. The solid was dissolved in acetone (50 mL) and [NBu^n_4]Cl in acetone was added to yield a cream-coloured precipitate which was filtered off, washed with acetone and dried. Yield: 488 mg (56%). δ_H (400 MHz, CD_3OD) 9.43 (4H, d, *J* = 7.1 Hz, C_5H_4N), 9.17 (2H, dd, *J* = 1.9, 0.9 Hz, C_5H_3N), 9.08 (2H, dd, *J* = 5.0, 0.8 Hz, C_5H_3N), 8.81 (4H, d, *J* = 7.1 Hz, C_5H_4N), 8.18 (2H, dd, *J* = 5.2, 1.9 Hz, C_5H_3N), 7.95–7.91 (4H, Ph), 7.83–7.79 (6H, Ph). *Anal.* Calc. (%) for $C_{32}H_{24}Cl_2N_4{\cdot}H_2O$: C, 69.44; H, 4.73; N, 10.12. Found: C, 69.14; H, 4.92; N, 10.04%. ES-MS: *m*/*z* = 499 ([M−Cl]$^+$), 232 ([M−2Cl]$^{2+}$).

2.2.4. *N*″,*N*‴-Di(4-acetylphenyl)-4,4′:2′,2″:4″,4‴-quaterpyridinium chloride, [$(4\text{-}AcPh)_2qpy^{2+}$]$Cl_2$

This compound was prepared in a manner similar to [Ph_2qpy^{2+}]Cl_2 by using 4-aminoacetophenone (4.01 g, 29.6 mmol) instead of aniline, and the mixture was heated at reflux in ethanol (50 mL) for 50 h. The resulting brown solution was reduced in volume and acetone (200 mL) was added to give a brown precipitate, [$(4\text{-}AcPh)_2qpy^{2+}$]$Cl_2$, which was filtered off. The solid was dissolved in water (100 mL) and extracted with chloroform (3 × 200 mL). Aqueous NH_4PF_6 was added to the aqueous layer yielding a pale brown precipitate, [$(4\text{-}AcPh)_2qpy^{2+}$][$PF_6$]$_2$, which was filtered off and dried. The solid was dissolved in acetone (70 mL) and filtered. [NBu^n_4]Cl in acetone was added to the filtrate to afford a pale brown solid which was filtered off, washed with acetone and dried. Yield: 448 mg (44%). δ_H (400 MHz, CD_3OD) 9.48 (4H, d, *J* = 7.1 Hz, C_5H_4N), 9.18 (2H, d, *J* = 1.3 Hz, C_5H_3N), 9.09 (2H, d, *J* = 5.3 Hz, C_5H_3N), 8.85 (4H, d, *J* = 7.1 Hz, C_5H_4N), 8.39 (4H, d, *J* = 8.8 Hz, C_6H_4), 8.19 (2H, dd, *J* = 5.0, 1.8 Hz, C_5H_3N), 8.07 (4H, d, *J* = 8.6 Hz, C_6H_4), 2.74 (6H, s, Me). ν(C=O) 1682s cm^{-1}. *Anal.* Calc. (%) for $C_{36}H_{28}Cl_2N_4O_4{\cdot}1.8H_2O$: C, 66.32; H, 4.89; N, 8.59. Found: C, 66.36; H, 4.92; N, 8.88%. ES-MS: *m*/*z* = 583 ([M−Cl]$^+$), 274 ([M−2Cl]$^{2+}$).

2.2.5. *N*″,*N*‴-Di(2-pyrimidyl)-4,4′:2′,2″:4″,4‴-quaterpyridinium chloride, [$(2\text{-}Pym)_2qpy^{2+}$]Cl_2

A mixture of qpy·0.5H_2O (500 mg, 1.57 mmol) and 2-chloropyrimidine (1.80 g, 15.7 mmol) was heated at 120 °C. Ethanol (15 mL)

was added to the resulting green solution and the mixture was heated at reflux for 4 h. The solution was allowed to cool and diethyl ether (100 mL) was added to give a pale brown precipitate, $[(2\text{-Pym})_2qpy^{2+}]Cl_2$, which was filtered off. The solid was dissolved in water and aqueous NH_4PF_6 was added to give a brown precipitate, $[(2\text{-Pym})_2qpy^{2+}][PF_6]_2$, which was filtered off and dried. The solid was dissolved in acetone (150 mL) and filtered. $[NBu^n_4]Cl$ in acetone was added to the filtrate to give a pale brown precipitate which was filtered off, washed with acetone and dried. Yield: 827 mg (91%). δ_H (400 MHz, CD_3OD) 10.33 (4H, d, J = 7.3 Hz, C_5H_4N), 9.22 (4H, d, J = 4.8 Hz, $C_4H_3N_2$), 9.21 (2H, d, J = 0.8 Hz, C_5H_3N), 9.10 (2H, dd, J = 5.3, 0.8 Hz, C_5H_3N), 8.90 (4H, d, J = 7.3 Hz, C_5H_4N), 8.21 (2H, dd, J = 5.2, 1.9 Hz, C_5H_3N), 7.94 (2H, t, J = 4.9 Hz, $C_4H_3N_2$). *Anal.* Calc. (%) for $C_{28}H_{20}Cl_2N_8{\cdot}2.3H_2O$: C, 57.90; H, 4.27; N, 19.29. Found: C, 57.87; H, 4.05; N, 19.12%. ES-MS: m/z = 503 ($[M-Cl]^+$), 234 ($[M-2Cl]^{2+}$).

2.2.6. N″,N‴-Di(2,4-dinitrophenyl)-4,4′:2′,2″:4″,4‴-quaterpyridinium chloride, $[(2,4\text{-DNPh})_2qpy^{2+}]Cl_2$

The reaction to prepare $[(2,4\text{-DNPh})_2qpy^{2+}]Cl_2$ was exactly as in the procedure for $[Ph_2qpy^{2+}]Cl_2$. The solution was allowed to cool and chloroform (20 mL) was added to produce a cream-coloured precipitate which was filtered off and washed with diethyl ether. Purification was effected by reprecipitation from MeOH/diethyl ether. Yield: 972 mg (85%). δ_H (400 MHz, CD_3OD) 9.48 (4H, d, J = 7.3 Hz, C_5H_4N), 9.33 (2H, d, J = 2.5 Hz, $C_6H_3N_2O_4$), 9.22 (2H, dd, J = 2.0, 0.8 Hz, C_5H_3N), 9.11 (2H, dd, J = 5.3, 0.8 Hz, C_5H_3N), 8.99–8.94 (6H, C_5H_4N + $C_6H_3N_2O_4$), 8.40 (2H, d, J = 8.6 Hz, $C_6H_3N_2O_4$), 8.23 (2H, dd, J = 5.2, 1.9 Hz, C_5H_3N). $\nu_{as}(NO_2)$ 1535vs, $\nu_s(NO_2)$ 1342vs cm^{-1}. *Anal.* Calc. (%) for $C_{32}H_{20}Cl_2N_8O_8{\cdot}0.5H_2O$: C, 53.05; H, 2.92; N, 15.47. Found: C, 53.24; H, 2.67; N, 15.01%. ES-MS: m/z = 679 ($[M-Cl]^+$), 322 ($[M-2Cl]^{2+}$).

2.2.7. N″,N‴-Di(3,5-bismethoxycarbonylphenyl)-4,4′:2′,2″:4″,4‴-quaterpyridinium chloride, $[(3,5\text{-}MC_2Ph)_2qpy^{2+}]Cl_2$

This compound was prepared in a manner similar to $[(4\text{-AcPh})_2qpy^{2+}]Cl_2$ by using dimethoxy-5-aminoisophthalate (3.27 g, 15.6 mmol) instead of 4-aminoacetophenone. The red/orange solution was evaporated to dryness and the solid was washed with acetone (150 mL) under filtration. The resulting yellow solid was dissolved in water (200 mL) and extracted with chloroform (3 × 200 mL). The aqueous layer was concentrated under vacuum. Acetone was added to the pale green solution, affording a cream-coloured precipitate which was filtered off, washed with acetone and dried. Yield: 876 mg (69%). δ_H (400 MHz, CD_3OD) 9.51 (4H, d, J = 7.1 Hz, C_5H_4N), 9.20 (2H, d, J = 1.3 Hz, C_5H_3N), 9.09 (2H, d, J = 5.3 Hz, C_5H_3N), 8.95 (2H, t, J = 1.5 Hz, C_6H_3), 8.86 (4H, d, J = 7.1 Hz, C_5H_4N), 8.78 (4H, d, J = 1.5 Hz, C_6H_3), 8.20 (2H, dd, J = 5.2, 1.9 Hz, C_5H_3N), 4.05 (12H, s, Me). ν(C=O) 1721s cm^{-1}. *Anal.* Calc. (%) for $C_{40}H_{32}Cl_2N_4O_8{\cdot}2H_2O$: C, 59.78; H, 4.52; N, 6.97. Found: C, 59.60; H, 4.31; N, 6.99%. ES-MS: m/z = 731 ($[M-Cl]^+$), 348 ($[M-2Cl]^{2+}$).

2.2.8. N″,N‴-Di(4-methoxycarbonylphenyl)-4,4′:2′,2″:4″,4‴-quaterpyridinium chloride, $[(4\text{-MCPh})_2qpy^{2+}]Cl_2$

This compound was prepared in a manner similar to $[(3,5\text{-}MC_2Ph)_2qpy^{2+}]Cl_2$ by using methyl-4-aminobenzoate (2.37 g, 15.7 mmol) instead of dimethoxy-5-aminoisophthalate, and a reflux time of 72 h. Reprecipitation from methanol/diethyl ether gave the pure product as a pale brown solid. Yield: 326 mg (29%). δ_H (400 MHz, CD_3OD) 9.48 (4H, d, J = 7.1 Hz, C_5H_4N), 9.18 (2H, d, J = 1.3 Hz, C_5H_3N), 9.09 (2H, dd, J = 5.2, 0.6 Hz, C_5H_3N), 8.85 (4H, d, J = 7.1 Hz, C_5H_4N), 8.41 (4H, d, J = 8.8 Hz, C_6H_4), 8.19 (2H, dd, J = 5.0, 2.0 Hz, C_5H_3N), 8.07 (4H, d, J = 8.8 Hz, C_6H_4), 4.01 (6H, s, Me). ν(C=O) 1720s cm^{-1}. *Anal.* Calc. (%) for $C_{36}H_{28}Cl_2N_4O_4{\cdot}3.5H_2O$: C, 60.51; H, 4.94; N, 7.84. Found: C, 60.40; H, 4.88; N, 7.75%. ES-MS: m/z = 615 ($[M-Cl]^+$), 290 ($[M-2Cl]^{2+}$).

2.2.9. cis-$[Ru^{II}(bpy)_2qpy][PF_6]_2$ (**1**)

A solution of *cis*-$Ru^{II}Cl_2(bpy)_2{\cdot}2H_2O$ (100 mg, 0.192 mmol) and $qpy{\cdot}0.5H_2O$ (61 mg, 0.191 mmol) in ethylene glycol (20 mL) was heated at reflux for 1 h. The dark red/orange solution was allowed to cool to room temperature and filtered. Aqueous NH_4PF_6 was added to the filtrate and a dark red precipitate was filtered off and washed with water. Purification was achieved by using a silica gel column, eluting with 0.3 M NH_4PF_6 in 1:1 acetone/acetonitrile to remove an initial orange band, then with 0.3 M NH_4PF_6 in acetone to remove the major red product band. The red fraction was evaporated to dryness, washed with water and dried to yield a bright orange solid. Yield: 92 mg (47%). δ_H (400 MHz, CD_3COCD_3) 9.43 (2H, d, J = 1.5 Hz, *a*), 8.85 (4H, d, J = 8.3 Hz, C_5H_4N), 8.81 (4H, d, J = 5.6 Hz, *b*), 8.26–8.21 (6H, py), 8.19–8.17 (2H, m, py), 8.10–8.08 (2H, m, py), 7.98 (2H, dd, J = 6.1, 2.0 Hz, py), 7.94 (4H, d, J = 6.3 Hz, C_5H_4N), 7.63–7.56 (4H, py). *Anal.* Calc. (%) for $C_{40}H_{30}F_{12}N_8P_2Ru{\cdot}H_2O$: C, 46.56; H, 3.13; N, 10.86. Found: C, 46.70; H, 2.82; N, 10.79%. MALDI-MS: m/z = 870 ($[M-PF_6]^+$), 725 ($[M-2PF_6]^+$).

2.2.10. cis-$[Ru^{II}(bpy)_2(Me_2qpy^{2+})][PF_6]_4$ (**2**)

This compound was prepared and purified in a manner similar to **1** by using $[Me_2qpy^{2+}]Cl_2{\cdot}3.1H_2O$ (79 mg, 0.169 mmol) instead of $qpy{\cdot}0.5H_2O$ and ethanol (50 mL) instead of ethylene glycol, with a reflux time of 2 h. The column was eluted with 0.1 M NH_4PF_6 in acetonitrile, and the first red band afforded a dark red solid. Yield: 114 mg (49%). δ_H (400 MHz, CD_3COCD_3) 9.48 (2H, d, J = 1.8 Hz, *a*), 9.21 (4H, d, J = 7.1 Hz, *b*), 8.85 (4H, d, J = 8.3 Hz, C_5H_4N), 8.71 (4H, d, J = 6.8 Hz, C_5H_4N), 8.40 (2H, d, J = 6.1 Hz, py), 8.28–8.22 (4H, m, C_5H_4N), 8.15–8.13 (4H, py), 8.07 (2H, dd, J = 5.6, 0.8 Hz, py), 7.64–7.60 (2H, m, py), 7.57–7.54 (2H, m, py), 4.69 (6H, s, Me). *Anal.* Calc. (%) for $C_{42}H_{36}F_{24}N_8P_4Ru{\cdot}3H_2O$: C, 36.35; H, 3.05; N, 8.07. Found: C, 36.39; H, 2.59; N, 8.02%. MALDI-MS: m/z = 1184 ($[M-PF_6]^+$), 1039 ($[M-2PF_6]^+$), 896 ($[M-3PF_6]^+$), 751 ($[M-4PF_6]^+$).

2.2.11. cis-$[Ru^{II}(bpy)_2(Ph_2qpy^{2+})][PF_6]_4$ (**3**)

This compound was prepared and purified in a manner similar to **2** by using *cis*-$Ru^{II}Cl_2(bpy)_2{\cdot}2H_2O$ (93 mg, 0.179 mmol) and $[Ph_2qpy^{2+}]Cl_2{\cdot}H_2O$ (96 mg, 0.173 mmol) instead of $[Me_2qpy^{2+}]Cl_2{\cdot}3.1H_2O$ to afford a dark red solid. Yield: 106 mg (41%). δ_H (400 MHz, CD_3COCD_3) 9.57 (2H, d, J = 1.8 Hz, *a*), 9.53 (4H, d, J = 7.1 Hz, *b*), 8.87 (8H, d, J = 7.1 Hz, C_5H_4N), 8.46 (2H, d, J = 6.1 Hz, py), 8.29–8.24 (4H, m, C_5H_4N), 8.22 (2H, dd, J = 6.0, 2.0 Hz, py), 8.17 (2H, dd, J = 5.6, 0.8 Hz, py), 8.09 (2H, dd, J = 5.7, 0.6 Hz, py), 8.00–7.98 (4H, Ph), 7.84–7.80 (6H, Ph), 7.66–7.62 (2H, m, py), 7.60–7.56 (2H, m, py). *Anal.* Calc. (%) for $C_{52}H_{40}F_{24}N_8P_4Ru{\cdot}2H_2O$: C, 41.81; H, 2.97; N, 7.50. Found: C, 41.81; H, 2.69; N, 7.37%. MALDI-MS: m/z = 1309 ($[M-PF_6]^+$), 1165 ($[M-2PF_6]^+$), 1021 ($[M-3PF_6]^+$), 878 ($[M-4PF_6]^+$).

All of the compounds **4**–**11** were prepared and purified in a manner similar to **2** by using the appropriate pro-ligand salt, giving dark red solids.

2.2.12. cis-$[Ru^{II}(bpy)_2\{(4\text{-AcPh})_2qpy^{2+}\}][PF_6]_4$ (**4**)

Used $[(4\text{-AcPh})_2qpy^{2+}]Cl_2{\cdot}1.8H_2O$ (119 mg, 0.183 mmol). Yield: 109 mg (38%). δ_H (400 MHz, CD_3COCD_3) 9.59 (4H, d, J = 7.1 Hz, *b*), 9.55 (2H, d, J = 1.8 Hz, *a*), 8.90–8.86 (8H, py), 8.46 (2H, d, J = 6.1 Hz, py), 8.37 (4H, d, J = 9.1 Hz, C_6H_4), 8.29–8.24 (4H, m, C_5H_4N), 8.22 (2H, dd, J = 6.0, 2.0 Hz, py), 8.18–8.14 (6H, py + C_6H_4), 8.09 (2H, dd, J = 5.6, 0.8 Hz, py), 7.66–7.62 (2H, m, py), 7.60–7.56 (2H, m, py), 2.72 (6H, s, Me). ν(C=O) 1680s cm^{-1}. *Anal.* Calc. (%) for $C_{56}H_{44}F_{24}N_8O_2P_4Ru{\cdot}2H_2O$: C, 42.62; H, 3.07; N, 7.10. Found: C,

42.52; H, 2.76; N, 7.07%. MALDI-MS: m/z = 1393 ($[M-PF_6]^+$), 1249 $[M-2PF_6]^+$), 1104 ($[M-3PF_6]^+$), 960 $[M-4PF_6]^+$).

*2.2.13. cis-[Ru^{II}(bpy)$_2${(2-Pym)$_2$qpy^{2+}}][PF$_6$]$_4$ (**5**)*

Used [(2-Pym)$_2$qpy^{2+}]Cl$_2$·2.3H$_2$O (104 mg, 0.179 mmol). Yield: 122 mg (46%). δ_H (400 MHz, CD_3COCD_3) 10.36 (4H, d, J = 7.6 Hz, *b*), 9.61 (2H, d, J = 1.5 Hz, *a*), 9.29 (4H, d, J = 4.8 Hz, $C_4H_3N_2$), 9.00 (4H, d, J = 7.6 Hz, C_5H_4N), 8.88 (4H, d, J = 8.3 Hz, C_5H_4N), 8.52 (2H, d, J = 6.1 Hz, py), 8.31–8.24 (6H, py), 8.19 (2H, dd, J = 5.8, 0.8 Hz, py), 8.10 (2H, dd, J = 5.8, 0.8 Hz, py), 8.05 (2H, t, J = 4.8 Hz, $C_4H_3N_2$), 7.67–7.63 (2H, m, py), 7.60–7.56 (2H, m, py). *Anal.* Calc. (%) for $C_{48}H_{36}F_{24}N_{12}P_4Ru{\cdot}2H_2O$: C, 38.49; H, 2.69; N, 11.22. Found: C, 38.41; H, 2.46; N, 10.89%. MALDI-MS: m/z = 1319 ($[M-PF_6]^+$), 1173 ($[M-2PF_6]^+$), 1029 ($[M-3PF_6]^+$), 884 ($[M-4PF_6]^+$).

*2.2.14. cis-[Ru^{II}(bpy)$_2${(2,4-DNPh)$_2$qpy^{2+}}][PF$_6$]$_4$ (**6**)*

Used [(2,4-DNPh)$_2$qpy^{2+}]Cl$_2$·0.5H$_2$O (138 mg, 0.190 mmol). Yield: 110 mg (34%). δ_H (400 MHz, CD_3COCD_3) 9.63 (2H, d, J = 1.8 Hz, *a*), 9.58 (4H, d, J = 7.1 Hz, *b*), 9.28 (2H, d, J = 2.5 Hz, C_6H_3), 9.05 (2H, dd, J = 8.6, 2.5 Hz, C_6H_3), 9.01 (4H, d, J = 7.1 Hz, C_5H_4N), 8.88 (4H, d, J = 8.1 Hz, C_5H_4N), 8.57 (2H, d, J = 8.6 Hz, C_6H_3), 8.53 (2H, d, J = 6.0 Hz, py), 8.30–8.25 (6H, py), 8.18 (2H, d, J = 5.6 Hz, py), 8.10 (2H, d, J = 5.3 Hz, py), 7.67–7.63 (2H, m, py), 7.61–7.58 (2H, m, py). $\nu_{as}(NO_2)$ 1543s, $\nu_s(NO_2)$ 1344s cm^{-1}. *Anal.* Calc. (%) for $C_{52}H_{36}F_{24}N_{12}O_8P_4Ru{\cdot}3H_2O$: C, 36.91; H, 2.50; N, 9.93. Found: C, 36.85; H, 2.12; N, 9.69%. MALDI-MS: m/z = 1487 ($[M-PF_6]^+$), 1342 ($[M-2PF_6]^+$), 1200 ($[M-3PF_6]^+$).

*2.2.15. cis-[Ru^{II}(bpy)$_2${(3,5-MC$_2$Ph)$_2$qpy^{2+}}][PF$_6$]$_4$ (**7**)*

Used [(3,5-MC$_2$Ph)$_2$qpy^{2+}]Cl$_2$·2H$_2$O (148 mg, 0.184 mmol). Yield: 159 mg (50%). δ_H (400 MHz, CD_3COCD_3) 9.68 (4H, d, J = 7.1 Hz, *b*), 9.55 (2H, d, J = 1.5 Hz, *a*), 8.94 (4H, d, J = 7.1 Hz, C_5H_4N), 8.88–8.85 (6H, C_5H_4N + C_6H_3), 8.80 (4H, d, J = 1.3 Hz, C_6H_3), 8.47 (2H, d, J = 6.1 Hz, py), 8.30–8.23 (6H, py), 8.18 (2H, dd, J = 5.8, 0.8 Hz, py), 8.09 (2H, dd, J = 5.8, 0.8 Hz, py), 7.66–7.63 (2H, m, py), 7.61–7.57 (2H, m, py), 4.00 (12H, s, Me). ν(C=O) 1717s cm^{-1}. *Anal.* Calc. (%) for $C_{60}H_{48}F_{24}N_8O_8P_4Ru{\cdot}2H_2O$: C, 41.75; H, 3.04; N, 6.49. Found: C, 41.97; H, 2.81; N, 6.42%. MALDI-MS: m/z = 1542 ($[M-PF_6]^+$), 1397 ($[M-2PF_6]^+$), 1253 ($[M-3PF_6]^+$), 1108 ($[M-4PF_6]^+$).

*2.2.16. cis-[Ru^{II}(bpy)$_2${(4-MCPh)$_2$qpy^{2+}}][PF$_6$]$_4$ (**8**)*

Used [(4-MCPh)$_2$qpy^{2+}]Cl$_2$·3.5H$_2$O (125 mg, 0.175 mmol). Yield: 154 mg (53%). δ_H (400 MHz, CD_3COCD_3) 9.59 (4H, d, J = 7.3 Hz, *b*), 9.55 (2H, d, J = 1.8 Hz, *a*), 8.90–8.86 (8H, C_5H_4N), 8.46 (2H, d, J = 6.1 Hz, py), 8.38 (4H, d, J = 8.8 Hz, C_6H_4), 8.29–8.24 (4H, m, C_5H_4N), 8.22 (2H, dd, J = 6.0, 2.0 Hz, py), 8.17–8.14 (6H, py + C_6H_4), 8.09 (2H, dd, J = 5.6, 0.8 Hz, py), 7.66–7.62 (2H, m, py), 7.60–7.57 (2H, m, py), 3.98 (6H, s, Me). ν(C=O) 1709s cm^{-1}. *Anal.* Calc. (%) for $C_{56}H_{44}F_{24}N_8O_4P_4Ru{\cdot}4H_2O$: C, 40.86; H, 3.18; N, 6.81. Found: C, 41.00; H, 2.76; N, 6.79%. MALDI-MS: m/z = 1427 ($[M-PF_6]^+$), 1284 ($[M-2PF_6]^+$), 1140 ($[M-3PF_6]^+$), 996 ($[M-4PF_6]^+$).

*2.2.17. cis-[Ru^{II}(bpy)$_2$(Me$_2$bbpe^{2+})][PF$_6$]$_4$ (**9**)*

Used [Me$_2$bbpe^{2+}]I$_2$·0.7H$_2$O (124 mg, 0.188 mmol). Yield: 62 mg (23%). δ_H (400 MHz, CD_3COCD_3) 9.06–9.05 (6H, py), 8.83 (4H, d, J = 8.1 Hz, C_5H_4N), 8.37 (4H, d, J = 6.8 Hz, C_5H_4N), 8.25–8.20 (4H, m, C_5H_4N), 8.18–8.16 (4H, py), 8.13 (2H, d, J = 16.4 Hz, CH), 8.06 (2H, dd, J = 5.8, 0.8 Hz, py), 8.00 (2H, d, J = 16.7 Hz, CH), 7.81 (2H, dd, J = 6.1, 1.8 Hz, py), 7.61–7.56 (4H, py), 4.60 (6H, s, Me). *Anal.* Calc. (%) for $C_{46}H_{40}F_{24}N_8P_4Ru{\cdot}2H_2O$: C, 38.86; H, 3.12; N, 7.88. Found: C, 39.00; H, 2.86; N, 7.80%. MALDI-MS: m/z = 1242 ($[M-PF_6]^+$), 1097 ($[M-2PF_6]^+$), 952 ($[M-3PF_6]^+$), 807 ($[M-4PF_6]^+$).

*2.2.18. cis-[Ru^{II}(bpy)$_2$(Ph$_2$bbpe^{2+})][PF$_6$]$_4$ (**10**)*

Used [Ph$_2$bbpe^{2+}]Cl$_2$·4.5H$_2$O (113 mg, 0.169 mmol). Yield: 143 mg (54%). δ_H (400 MHz, CD_3COCD_3) 9.38 (4H, d, J = 7.1 Hz, *b*), 9.12 (2H, d, J = 1.5 Hz, *a*), 8.85 (4H, d, J = 8.2 Hz, C_5H_4N), 8.54 (4H, d, J = 7.1 Hz, C_5H_4N), 8.29–8.20 (10H, py + CH), 8.12 (2H, d, J = 16.4 Hz, CH), 8.07 (2H, dd, J = 5.6, 0.8 Hz, py), 8.03–8.01 (4H, Ph), 7.87 (2H, dd, J = 6.1, 1.8 Hz, py), 7.83–7.79 (6H, Ph), 7.63–7.58 (4H, py). *Anal.* Calc. (%) for $C_{56}H_{44}F_{24}N_8P_4Ru{\cdot}3H_2O$: C, 43.01; H, 3.22; N, 7.16. Found: C, 43.08; H, 2.83; N, 7.00%. MALDI-MS: m/z = 1365 ($[M-PF_6]^+$), 1220 ($[M-2PF_6]^+$), 1075 ($[M-3PF_6]^+$), 931 ($[M-4PF_6]^+$).

*2.2.19. cis-[Ru^{II}(bpy)$_2${(2,4-DNPh)$_2$bbpe^{2+}}][PF$_6$]$_4$ (**11**)*

Used [(2,4-DNPh)$_2$bbpe^{2+}]Cl$_2$·3.8H$_2$O (148 mg, 0.177 mmol). Yield: 106 mg (35%). δ_H (400 MHz, CD_3COCD_3) 9.40 (4H, d, J = 7.1 Hz, *b*), 9.27 (2H, d, J = 2.5 Hz, C_6H_3), 9.13 (2H, d, J = 1.3 Hz, *a*), 9.04 (2H, dd, J = 8.6, 2.5 Hz, C_6H_3), 8.85 (4H, d, J = 7.8 Hz, C_5H_4N), 8.65–8.63 (6H, py + C_6H_3), 8.35 (2H, d, J = 16.4 Hz, CH), 8.27–8.20 (8H, py), 8.16 (2H, d, J = 16.4 Hz, CH), 8.08 (2H, dd, J = 5.6, 0.8 Hz, py), 7.88 (2H, dd, J = 6.1, 1.8 Hz, py), 7.63–7.58 (4H, py). $\nu_{as}(NO_2)$ 1545s, $\nu_s(NO_2)$ 1344s cm^{-1}. *Anal.* Calc. (%) for $C_{56}H_{40}F_{24}N_{12}O_8P_4Ru{\cdot}2H_2O$: C, 38.97; H, 2.57; N, 9.74. Found: C, 38.84; H, 2.41; N, 9.50%. MALDI-MS: m/z = 1546 ($[M-PF_6]^+$), 1401 ($[M-2PF_6]^+$).

*2.2.20. cis-[Ru^{II}(bpy)$_2${[3,5-(CO$_2$H)$_2$Ph]$_2$qpy^{2+}}][PF$_6$]$_4$ (**12**)*

7.2H$_2$O (159 mg, 0.092 mmol) was dissolved in acetone (15 mL) and [NBu$^n_4$]Cl in acetone was added to give *cis*-[Ru^{II}(bpy)$_2${(3,5-MC$_2$Ph)$_2$qpy^{2+}}]Cl$_4$ (141 mg), which was filtered off. 100 mg of the latter material was added to *tert*-butanol (25 mL), followed by concentrated H_2SO_4 (1 mL), and the mixture was heated at reflux for 24 h. After cooling, aqueous NH_4PF_6 was added to afford a dark red solid which was filtered off, washed with water and dried. Yield: 86 mg (80%). δ_H (400 MHz, CD_3COCD_3) 9.72 (4H, d, J = 7.1 Hz, *b*), 9.61 (2H, d, J = 1.8 Hz, *a*), 8.96 (4H, d, J = 7.1 Hz, C_5H_4N), 8.92 (2H, t, J = 1.4 Hz, C_6H_3), 8.88 (4H, d, J = 8.3 Hz, C_5H_4N), 8.79 (4H, d, J = 1.5 Hz, C_6H_3), 8.48 (2H, d, J = 6.1 Hz, py), 8.30–8.25 (6H, py), 8.18 (2H, d, J = 5.6 Hz, py), 8.09 (2H, dd, J = 5.7, 0.9 Hz, py), 7.67–7.63 (2H, m, py), 7.61–7.57 (2H, m, py). ν(C=O) 1713s cm^{-1}. *Anal.* Calc. (%) for $C_{56}H_{40}F_{24}N_8O_8P_4Ru$: C, 41.16; H, 2.47; N, 6.86. Found: C, 41.40; H, 2.70; N, 6.48%. MALDI-MS: m/z = 1344 ($[M-2PF_6]^+$), 1199 ($[M-3PF_6]^+$), 1055 ($[M-4PF_6]^+$).

*2.2.21. cis-[Ru^{II}(bpy)$_2${[4-(CO$_2$H)Ph]$_2$qpy^{2+}}][PF$_6$]$_4$ (**13**)*

This compound was prepared in a manner similar to **12** by converting **8**.4H$_2$O (154 mg, 0.094 mmol) into *cis*-[Ru^{II}(bpy)$_2${(4-MCPh)$_2$qpy^{2+}}]Cl$_4$ (118 mg), and hydrolysing 100 mg of this material. The resulting dark red solid was purified by reprecipitation from acetone/diethyl ether. Yield: 85 mg (69%). δ_H (400 MHz, CD_3COCD_3) 9.64 (2H, s, *a*), 9.60 (4H, d, J = 6.8 Hz, *b*), 8.95 (4H, d, J = 6.8 Hz, C_5H_4N), 8.88 (4H, d, J = 8.3 Hz, C_5H_4N), 8.47 (2H, d, J = 6.3 Hz, py), 8.39 (4H, d, J = 8.6 Hz, C_6H_4), 8.30–8.24 (6H, py), 8.19–8.14 (6H, py + C_6H_4), 8.09 (2H, d, J = 5.0 Hz, py), 7.66–7.63 (2H, m, py), 7.60–7.57 (2H, m, py). ν(C=O) 1703s cm^{-1}. *Anal.* Calc. (%) for $C_{54}H_{40}F_{24}N_8O_4P_4Ru$: C, 41.95; H, 2.61; N, 7.25. Found: C, 42.32; H, 2.45; N, 7.24%. MALDI-MS: m/z = 1401 ($[M-PF_6]^+$), 1256 ($[M-2PF_6]^+$), 1112 ($[M-3PF_6]^+$), 967 ($[M-4PF_6]^+$).

2.3. X-ray crystallography

Crystals of [(3,5-MC$_2$Ph)$_2$qpy^{2+}]Cl$_2$·5CD$_3$OD were grown by slow evaporation of a CD_3OD solution in an NMR tube, while those of complex salts **5**·2.75MeCN, **7**·2.5MeCN and **10**·2MeCN were obtained by vapour diffusion of diethyl ether into acetonitrile solutions. Data were collected on a Bruker APEX CCD X-ray diffractometer by using

Mo Kα radiation (λ = 0.71073 Å), and the data were processed by using the Bruker SAINT [14] and SADABS [15] software packages. The structures were solved by direct methods using SHELXS-97 [16], and refined by full-matrix least-squares on all F_0^2 data using SHELXL-97 [17]. All non-hydrogen atoms were refined anisotropically and hydrogen atoms were included in idealised positions using the riding model, with thermal parameters of 1.2 times those of aromatic parent carbon atoms, and 1.5 times those of methyl parent carbons.

The asymmetric unit of $[(3,5\text{-}MC_2Ph)_2qpy^{2+}]Cl_2\cdot 5CD_3OD$ contains half the cation and one Cl^- anion, together with one ordered and 3 disordered CD_3OD molecules, the latter at 0.5 occupancy. The asymmetric unit of **5**·2.75MeCN contains one cation and three whole and two half PF_6^- anions, with several MeCN molecules, one of which is at 0.75 occupancy. In one of the half PF_6^- anions, the P atom lies on a centre of symmetry and in the other, the F atoms are disordered over two sites each. Restraints were applied to the geometry and atomic displacement parameters (adps) of the disordered PF_6^- and some of the MeCN molecules. The asymmetric unit of **7**·2.5MeCN contains one cation, four PF_6^- anions and 2.5 MeCN molecules. Restraints were applied to the anisotropic adps and to the geometry of three of the PF_6^- ions and two of the MeCN molecules. The crystal diffracted very weakly so the data were cut at 1.1 Å resolution. For **10**·2MeCN, there are two cations in the asymmetric unit, and seven whole (one of which is disordered over two sites) and two half PF_6^- anions (the latter with the P atoms on 2-fold axes), as well as a number of MeCN molecules, some at 0.5 occupancy. Restraints were applied to the geometry of the disordered PF_6^- and to the partially occupied MeCN molecules, as well as the anisotropic adps. The data were cut at 1.05 Å because the crystal did not diffract beyond this resolution. All other calculations were carried out by using the SHELXTL package [18]. Crystallographic data and refinement details are presented in Table 1.

3. Results and discussion

3.1. Synthesis and characterisation

We have studied previously a number of salts of Ru^{II} complexes containing three bpy-based ligands bearing two electron-accepting pyridinium substituents, primarily for their interesting NLO properties [9–11,13]. The complex salts *cis*-$[Ru^{II}(bpy)_2qpy][PF_6]_2$ (**1**) [19] and *cis*-$[Ru^{II}(bpy)_2(Me_2qpy^{2+})][PF_6]_4$ (**2**) [19a,b] (Fig. 1) have been reported previously, but were obtained in this study *via* slightly modified methods. The new asymmetric complexes in salts **3**–**11** (Fig. 1) were prepared in part to allow comparisons of optical and redox properties with the symmetric tris-chelates, but also in order to access the potential photosensitizers **12** and **13**.

The compound 4,4′:2′,2″:4″,4‴-quaterpyridyl (qpy) was synthesised by combining a previously reported method [9], with the chromatographic purification described in another report [20], avoiding a prolonged Soxhlet extraction. Although this method is relatively convenient, a much higher yield (79%) of qpy has been obtained by Ni^0-mediated reductive coupling of 4-(2-chloropyridin-4-yl)pyridine [20]. While the *N*″,*N*‴-dimethyl-4,4′:2′,2″:4″,4‴-quaterpyridinium (Me_2qpy^{2+}) dication has been reported as its iodide and hexafluorophosphate salts [21], the chloride salt $[Me_2qpy^{2+}]Cl_2$ is to our knowledge a new compound. Because the salts $[Ph_2qpy^{2+}]Cl_2$, $[(4\text{-}AcPh)_2qpy^{2+}]Cl_2$, $[(2\text{-}Pym)_2qpy^{2+}]Cl_2$, $[(3,5\text{-}MC_2Ph)_2qpy^{2+}]Cl_2$ and $[(2,4\text{-}DNPh)_2qpy^{2+}]Cl_2$ were treated as intermediates in previous work [9,10], no analytical data were obtained. Such data together with modified synthetic methods for these compounds are hence included here. The new pro-ligand salt $[(4\text{-}MCPh)_2qpy^{2+}]Cl_2$ was synthesised in a manner similar to that used for its close relatives, *via* a Zincke-type reaction between $[(2,4\text{-}DNPh)_2qpy^{2+}]Cl_2$ and methyl-4-aminobenzoate.

The new complexes in **2**–**11** were prepared by reacting *cis*-$Ru^{II}Cl_2(bpy)_2\cdot 2H_2O$ with a little less than one equivalent of the appropriate pro-ligand chloride salt (except for Me_2bbpe^{2+} where the iodide salt was used) in ethanol under reflux. Yields in the range *ca.* 30–55% were obtained after purification on silica gel columns eluting with 0.1 M NH_4PF_6 in acetonitrile. It is perhaps significant that a relatively low yield (23%) was obtained when using the pro-ligand iodide salt to prepare the complex salt **9**. The carboxylate-substituted complex salts **12** and **13** were prepared in good yields simply *via* acid-catalysed hydrolysis of the methyl ester groups in **7** and **8**, respectively.

The identities and purities of all the products are confirmed by clean ^1H NMR spectra, together with +electrospray or MALDI mass spectra, CHN elemental analyses and IR spectra in cases where es-

Table 1
Crystallographic data and refinement details for the pro-ligand salt $[(3,5\text{-}MC_2Ph)_2qpy^{2+}]Cl_2\cdot 5CD_3OD$ and the complex salts **5**·2.75MeCN, **7**·2.5MeCN and **10**·2MeCN.

	$[(3,5\text{-}MC_2Ph)_2qpy^{2+}]Cl_2\cdot 5CD_3OD$	**5**·2.75MeCN	**7**·2.5MeCN	**10**·2MeCN
Formula	$C_{45}H_{32}Cl_2D_{20}N_4O_{13}$	$C_{53.5}H_{44.25}F_{24}N_{14.75}P_4Ru$	$C_{65}H_{55.5}F_{24}N_{10.5}O_8P_4Ru$	$C_{60}H_{50}F_{24}N_{10}P_4Ru$
Molecular weight	947.85	1574.74	1792.65	1592.05
Crystal system	monoclinic	triclinic	monoclinic	monoclinic
Space group	$P2_1/c$	$P\bar{1}$	$P2_1/c$	$C2/c$
a (Å)	8.6247(19)	13.947(2)	12.0679(17)	27.702(8)
b (Å)	24.445(5)	14.698(2)	13.4767(19)	36.615(10)
c (Å)	10.939(2)	18.064(2)	44.274(6)	26.253(8)
α (°)	90	90.699(3)	90	90
β (°)	91.712(4)	106.388(3)	90.886(3)	90.356(6)
γ (°)	90	117.404(2)	90	90
U (Å^3)	2305.3(9)	3100.1(8)	7199.7(17)	26628(13)
Z	2	2	4	16
D_{calc} (mg m^{-3})	1.365	1.687	1.654	1.588
T (K)	100(2)	100(2)	100(2)	100(2)
μ (mm^{-1})	0.209	0.481	0.431	0.447
Crystal size (mm)	0.30 × 0.20 × 0.10	0.30 × 0.20 × 0.20	0.40 × 0.30 × 0.05	0.65 × 0.30 × 0.05
Crystal appearance	pale yellow block	red block	red block	red plate
Reflections collected	12987	19351	27875	57217
Independent reflections (R_{int})	4711 (0.0601)	8889 (0.0667)	5648 (0.1160)	12038 (0.1644)
θ_{max}/° (completeness)	26.43 (99.2%)	23.26 (99.7%)	18.85 (99.9%)	19.78 (99.9%)
Reflections with $I > 2\sigma(I)$	2516	6547	4401	8044
Goodness-of-fit on F^2	0.726	1.089	1.725	1.120
Final R_1, wR_2 [$I > 2\sigma(I)$] (all data)	0.0494, 0.1073	0.0930, 0.2274	0.1634, 0.4085	0.1100, 0.2335
	0.1027, 0.1237	0.1251, 0.2471	0.1865, 0.4231	0.1568, 0.2570
Peak and hole (eÅ^{-3})	0.301, −0.269	1.640, −0.747	1.179, −1.466	1.030, −0.615

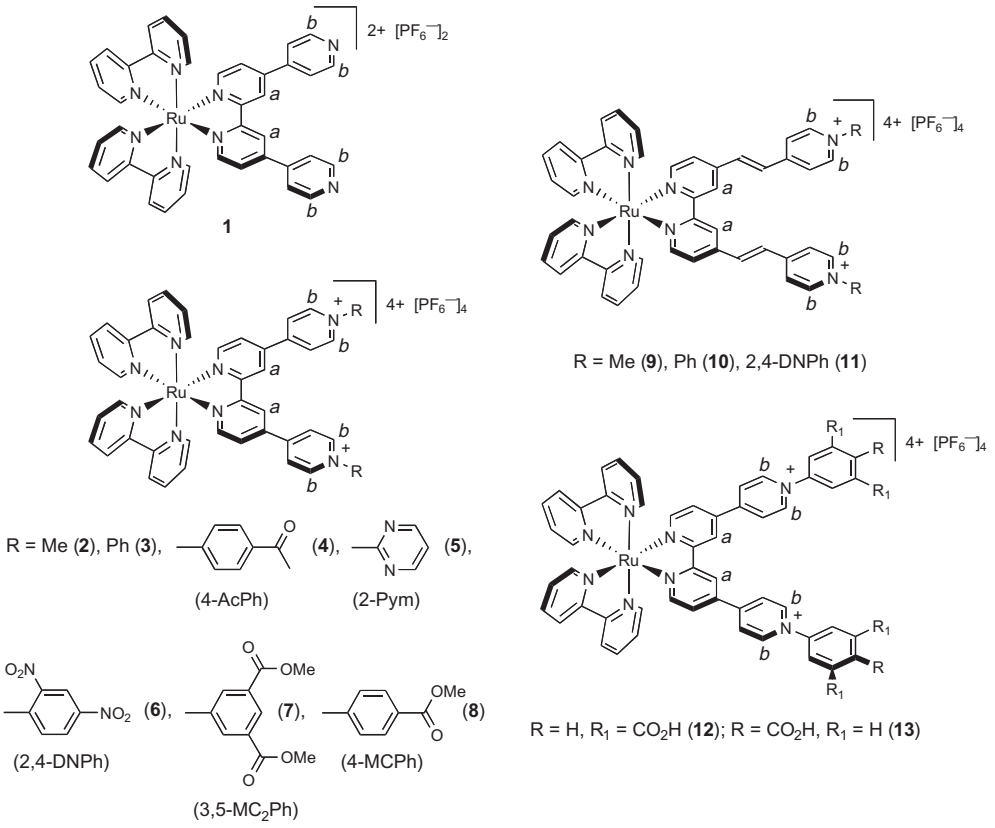

Fig. 1. Chemical structures of the Ru^{II} complex salts investigated, including the labelling for selected protons for which the signals are assigned in the ^1H NMR spectra.

ter, carboxylate or nitro functional groups are present. As is commonly the case for organic salts, all of the products contain residual water that is not removed by drying under vacuum at room temperature (the samples were not heated in order to avoid any possible decomposition).

3.2. ^1H NMR spectroscopy studies

While the relative complexity of the ^1H spectra precludes definitive assignment of many of the signals due to pyridyl ring protons (with a total of 30 in each compound), some of these signals can be attributed unambiguously to certain environments. In particular, a finely split doublet (J = 1.5 Hz, in all cases expect **13** for which the splitting is not resolved) to relatively low field and integrating for two protons must arise from the 3,3′-positions on the substituted bpy ligand (denoted *a*, Fig. 1). The position of this signal is logically sensitive to the adjacent substituents, and shows a downfield shift of 0.2 ppm on moving from **1** to **6** (Fig. 2), reflecting a substantial deshielding effect of the R substituent. Based on the chemical shift of this signal, the electron-withdrawing strength of R in the qpy-based complexes appears to be Me < 4-AcPh = 4-MCPh = 3,5-MC_2Ph < Ph < 2-Pym < 2,4-DNPh. This ordering correlates somewhat with that inferred previously from the MLCT absorption energies for the symmetric complexes $[Ru^{II}(R_2qpy^{2+})_3]^{8+}$, that show a significant difference between R = Me and Ph, but then little further change on moving to R = 4-AcPh or 3,5-MC_2Ph [10]. While the *a* proton signal is not resolved in the spectrum of **9** in CD_3COCD_3, for **10** and **11** it appears to high field by *ca.* 0.3 ppm when compared with **1**. This observation shows that the electron-donating (thus shielding) influence of the ethenylene units in **10** and **11** offsets considerably the deshielding effect of the pyridyl groups. Also, the fact that the *a* proton signal occurs at almost identical δ values in **10** and **11** shows that extending the conjugated systems lessens the influence of the pyridinium groups.

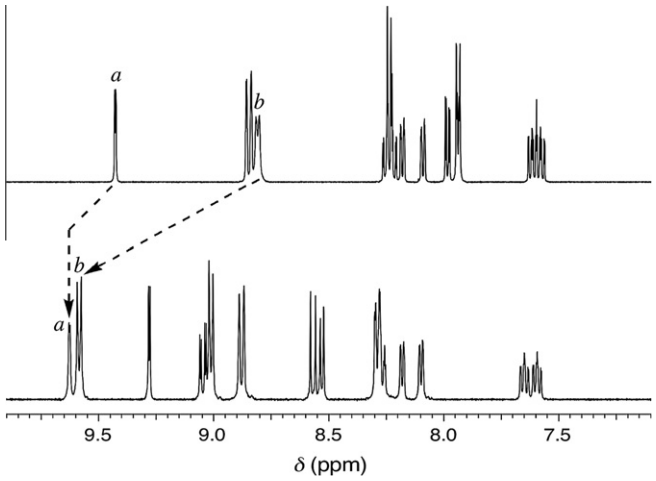

Fig. 2. Aromatic regions of the ^1H NMR spectra of the complex salts **1** (top) and **6** (bottom) recorded at 400 MHz in CD_3COCD_3 at 293 K. The arrows indicate the large downfield shifts observed for the *a* and *b* proton signals on quaternisation of the N atoms.

Any signal that shows a clear multiplet splitting and integrates for four protons can not be due to the C_5H_3N units, but rather must arise from the C_5H_4N groups. Although "C_5H_4N" can relate to the protons of the unsubstituted bpy ligands or the pendent/quaternised pyridyl rings, the lowest field four proton doublet (denoted *b*, Fig. 1) signals are almost certainly due to the protons adjacent to the deshielding quaternised N atoms. In **1**, this signal occurs to slightly higher field when compared with another four proton dou-

Table 2
UV–Vis absorption and electrochemical data for complex salts **1–13** in acetonitrile.

Salt	λ_{max}, nm (ε, 10^3 M^{-1} cm^{-1})[a]	E_{max} (eV)	Assignment	$E_{1/2}$ or E, V versus Ag–AgCl (ΔE_p, mV)[b]	
				$[E_{1/2}]Ru^{III/II}$	Reductions
1	463 (13.4)	2.68	$d \rightarrow \pi^*$	1.36 (90)	−1.11 (70)
	358 (9.9)	3.46	$d \rightarrow \pi^*$		−1.43 (80)
	288 (58.5)	4.31	$\pi \rightarrow \pi^*$		−1.64 (80)
	247 (46.2)	5.02	$\pi \rightarrow \pi^*$		
2[c]	500 (20.9)	2.48	$d \rightarrow \pi^*$	1.41 (80)	−0.70 (180)[d]
	428 (24.1)	2.90	$d \rightarrow \pi^*$		−1.19 (80)
	325 (27.5)	3.82	$\pi \rightarrow \pi^*$		−1.42 (90)
	284 (84.6)	4.37	$\pi \rightarrow \pi^*$		−1.59 (95)
	255 (72.6)	4.86	$\pi \rightarrow \pi^*$		
3[e]	507 (19.8)	2.45	$d \rightarrow \pi^*$	1.43 (80)	−0.54 (150)[d]
	433 (21.6)	2.86	$d \rightarrow \pi^*$		−0.98[f]
	334 (27.0)	3.71	$\pi \rightarrow \pi^*$		−1.06[g]
	285 (87.9)	4.35	$\pi \rightarrow \pi^*$		−1.14[f]
	256 (54.2)	4.84	$\pi \rightarrow \pi^*$		−1.24[g]
					−1.68[g]
4	507 (18.8)	2.45	$d \rightarrow \pi^*$	1.43 (75)	−0.54[g]
	436 (19.4)	2.84	$d \rightarrow \pi^*$		−0.79[g]
	337 (22.8)	3.68	$\pi \rightarrow \pi^*$		
	285 (84.6)	4.35	$\pi \rightarrow \pi^*$		
	256 (50.1)	4.84	$\pi \rightarrow \pi^*$		
5	512 (26.9)	2.42	$d \rightarrow \pi^*$	1.43 (80)	−0.26[f]
	439 (24.4)	2.82	$d \rightarrow \pi^*$		−0.36[g]
	341 (21.1)	3.64	$\pi \rightarrow \pi^*$		−0.80 (80)
	285 (129.0)	4.35	$\pi \rightarrow \pi^*$		−1.02[f]
	260 (61.6)	4.77	$\pi \rightarrow \pi^*$		−1.04[g]
					−1.26[f]
					−1.44[g]
6	512 (18.9)	2.42	$d \rightarrow \pi^*$	1.44 (80)	−0.66[g]
	438 (17.6)	2.83	$d \rightarrow \pi^*$		−0.92[g]
	340 (15.8)	3.65	$\pi \rightarrow \pi^*$		−1.25[g]
	283 (86.7)	4.38	$\pi \rightarrow \pi^*$		
	258 (69.0)	4.81	$\pi \rightarrow \pi^*$		
7	509 (27.5)	2.44	$d \rightarrow \pi^*$	1.44 (70)	−0.42[f]
	435 (28.5)	2.85	$d \rightarrow \pi^*$		−0.53[g]
	335 (28.3)	3.70	$\pi \rightarrow \pi^*$		−0.86[f]
	285 (123.0)	4.35	$\pi \rightarrow \pi^*$		−0.82[g]
	257 (74.6)	4.82	$\pi \rightarrow \pi^*$		−1.28[f]
					−1.42[f]
					−1.55[g]
					−1.68[f]
					−1.75[g]
					−1.91[g]
8	509 (23.0)	2.44	$d \rightarrow \pi^*$	1.43 (70)	−0.45[f]
	436 (23.8)	2.84	$d \rightarrow \pi^*$		−0.53[g]
	338 (26.1)	3.67	$\pi \rightarrow \pi^*$		−0.86[f]
	285 (117.0)	4.35	$\pi \rightarrow \pi^*$		−0.94[g]
	258 (63.8)	4.81	$\pi \rightarrow \pi^*$		−1.36[f]
					−1.48[g]
					−1.58[g]
					−1.64[f]
					−1.72[g]
9	497 (19.5)	2.49	$d \rightarrow \pi^*$	1.34 (60)	−0.68[g]
	439 (20.7)	2.82	$d \rightarrow \pi^*$		−0.99[g]
	342 (31.1)	3.63	$\pi \rightarrow \pi^*$		−1.29[f]
	288 (76.1)	4.31	$\pi \rightarrow \pi^*$		−1.34[g]
					−1.63[g]
10	502 (25.4)	2.47	$d \rightarrow \pi^*$	1.36 (85)	−0.53[g]
	445 (25.2)	2.79	$d \rightarrow \pi^*$		−1.17[g]
	324 (64.9)	3.83	$\pi \rightarrow \pi^*$		−1.25[f]
	289 (74.0)	4.29	$\pi \rightarrow \pi^*$		−1.31[g]
11	509 (29.4)	2.44	$d \rightarrow \pi^*$	1.36 (75)	−0.52[g]
	450 (25.8)	2.76	$d \rightarrow \pi^*$		−1.35[g]
	321 (75.8)	3.86	$\pi \rightarrow \pi^*$		
	288 (87.7)	4.31	$\pi \rightarrow \pi^*$		
12	511 (19.0)	2.43	$d \rightarrow \pi^*$	1.44 (80)	−0.52[g]
	438 (18.1)	2.83	$d \rightarrow \pi^*$		−0.61[f]
	335 (20.7)	3.70	$\pi \rightarrow \pi^*$		−1.01[g]
	286 (74.1)	4.33	$\pi \rightarrow \pi^*$		−1.04[f]
	256 (46.1)	4.84	$\pi \rightarrow \pi^*$		−1.45[f]
					−1.61[g]
13	509 (20.9)	2.44	$d \rightarrow \pi^*$	1.44 (90)	−0.53[g]
	435 (21.7)	2.85	$d \rightarrow \pi^*$		−0.57[f]
	335 (25.1)	3.70	$\pi \rightarrow \pi^*$		−0.89[g]

Table 2 (*continued*)

Salt	λ_{max}, nm (ε, 10^3 M^{-1} cm^{-1})[a]	E_{max} (eV)	Assignment	$E_{1/2}$ or E, V versus Ag–AgCl (ΔE_p, mV)[b]	
				$[E_{1/2}]Ru^{III/II}$	Reductions
	285 (91.8)	4.35	$\pi \rightarrow \pi^*$		−1.00[f]
	256 (52.3)	4.84	$\pi \rightarrow \pi^*$		−1.04[g]
					−1.45[f]
					−1.62[g]

[a] Solutions *ca.* 3–5 × 10^{-5} M.
[b] Measured in solutions *ca.* 10^{-3} M in analyte and 0.1 M in $[NBu^n_4]PF_6$ at a 2 mm disc glassy carbon working electrode with a scan rate of 200 mV s^{-1}. Ferrocene internal reference $E_{1/2}$ = 0.44 V, ΔE_p = 70–90 mV.
[c] Differential pulse voltammetry data, *V* versus Ag–AgCl (potential increment = 4 mV; amplitude = 50 mV; pulse width = 0.01 s): −0.62, −0.73, −1.17, −1.39, −1.58.
[d] Two strongly overlapped waves.
[e] Differential pulse voltammetry data, *V* versus Ag–AgCl (parameters as for **2**): −0.49, −0.56, −1.00, −1.18, −1.61.
[f] E_{pa} for an irreversible reduction process.
[g] E_{pc} for an irreversible reduction process.

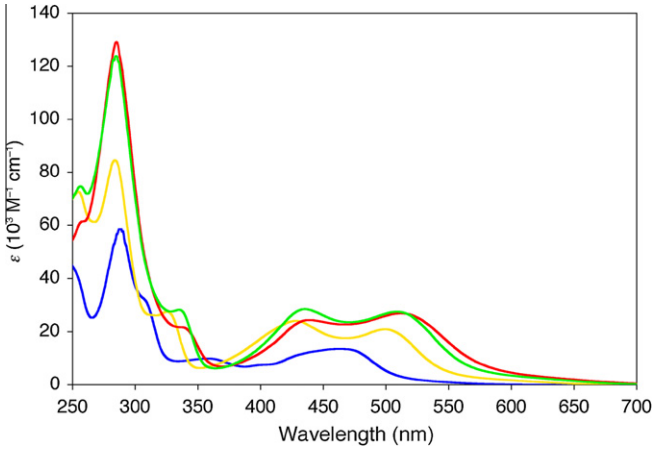

Fig. 3. UV–Vis absorption spectra of the complex salts **1** (blue), **2** (gold), **5** (red) and **7** (green) in acetonitrile at 293 K (Colour online).

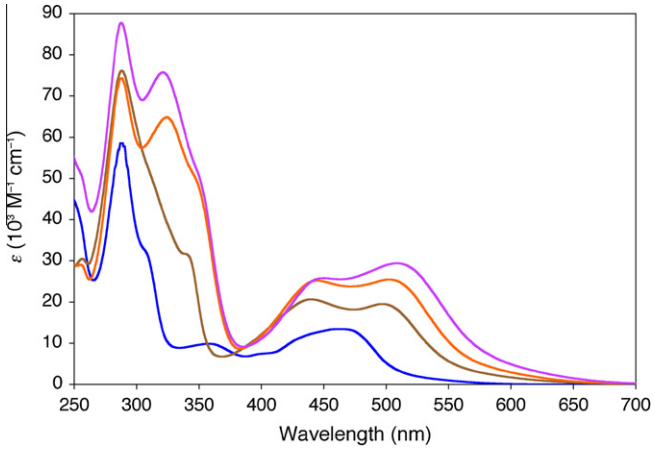

Fig. 4. UV–Vis absorption spectra of the complex salts **1** (blue), **9** (brown), **10** (orange) and **11** (purple) in acetonitrile at 293 K (Colour online).

blet that is attributable, based on its generally relatively large *J* value and near constancy in all of the spectra, to the bpy ligands. COSY experiments provide further confirmation of these assignments. As expected, the *b* proton signal shows pronounced sensitivity to the R group, with downfield shifts of *ca.* 0.8 ppm on moving from **1** to **6** (Fig. 2), and *ca.* 1.5 ppm on moving from **1** to **5**. Based on the δ value of this signal, the electron-withdrawing ordering for the qpy-based complexes is R = Me < Ph < 2,4-DNPh ≈ 4-AcPh = 4-MCPh < 3,5-MC_2Ph < 2-Pym. This ordering is clearly similar to, but not the same as, that indicated by the *a* proton signal (see above). Other ^{1}H NMR studies with $\{Ru^{II}(NH_3)_5\}^{2+}$ or *trans*-$\{Ru^{II}Cl(pdma)_2\}^+$ [pdma = 1,2-phenylenebis(dimethylarsine)] complexes of related monodentate 4,4′-bipyridinium ligands indicate the same (albeit incomplete) electron-withdrawing order R = Me < Ph < 2,4-DNPh < 4-AcPh < 2-Pym, based on the chemical shift of the *b* proton signal [22,23].

Where resolved, the ^{1}H signals observed for the phenyl/2-pyrimidyl rings or ethenylene groups can be assigned based on their coupling constants and multiplicities. The *J* values of *ca.* 16.5 Hz for the ethenylene signals in **9**–**11** confirm the presence of only the expected *E*-configurations in all cases.

3.3. Electronic spectroscopy studies

The UV–Vis absorption spectra of complex salts **1**–**13** have been measured in acetonitrile and the results are presented in Table 2. Representative spectra are shown in Figs. 3 and 4.

The spectra of complex salts **2**–**13** feature intense intraligand $\pi \rightarrow \pi^*$ absorptions in the UV region and also visible MLCT bands with two distinct maxima. A simplistic view might suggest that the high energy band corresponds with Ru → bpy MLCT, while the low energy band arises from Ru → L^A (L^A = a pyridinium-substituted bpy derivative) MLCT. However, the previously studied complexes $[Ru^{II}(L^A)_3]^{8+}$ also show two resolved bands [10,13] and both empirical trends and density functional theoretical calculations indicate that these derive from MLCT to the bpy and pyridinium units, with the latter transitions correlating with the higher energy (HE) bands [10]. Given that the E_{max} value for the HE band in **2**–**13** changes by only 0.07 eV when R is changed, while the lower energy (LE) band E_{max} varies more (by 0.14 eV), it seems likely that the latter still involves MLCT transitions to the pyridinium units. However, lowering the symmetry of the complexes complicates their electronic structures, so the observed bands may correspond with more than two transitions. In contrast, the spectrum of **1** shows only one visible maximum (with a poorly defined shoulder to high energy) which is markedly less intense than those of **2**–**13** (Figs. 3 and 4).

The visible E_{max} data obtained for **1** and **2** (Table 2) are very similar to those reported previously [19b], although the LE MLCT bands do show small solvatochromic shifts when measured in methanol [19a]. In contrast, the relative band intensities that we have measured differ from those published; Bierig et al. claimed that the MLCT band for **1** is more intense when compared with that for **2** [19a], while Hayes et al. reported very similar ε values for both compounds [19b]. The E_{max} value of the LE MLCT band in **2**–**13** is decreased by as much as *ca.* 0.26 eV when compared with that of **1**. Hence, it is clear that incorporating electron-accepting

Table 3
Low energy MLCT absorption and electrochemical data for tris-chelates $[Ru^{II}(R_2qpy^{2+})_3][PF_6]_8$ in acetonitrile.[a]

Salt	λ_{max}, nm (ε, 10^3 M^{-1} cm^{-1})[b]	E_{max} (eV)	$E_{1/2}$ or E, V versus Ag–AgCl (ΔE_p, mV)[c]	
			$[E_{1/2}]Ru^{III/II}$	Reduction
$[Ru^{II}(Me_2qpy^{2+})_3][PF_6]_8$	486 (37.3)	2.55	1.61 (110)	−0.69 (140)
	394 (26.4)	3.15		
$[Ru^{II}(Ph_2qpy^{2+})_3][PF_6]_8$	496 (37.3)	2.50	1.62 (110)	−0.52 (90)
	410 (26.1)	3.02		
$[Ru^{II}\{(4\text{-}AcPh)_2qpy^{2+}\}_3][PF_6]_8$	498 (49.5)	2.49	1.64 (180)[d]	−0.44[e]
	416 (33.5)	2.98		
$[Ru^{II}\{(3,5\text{-}MC_2Ph)_2qpy^{2+}\}_3][PF_6]_8$	498 (53.8)	2.49	1.65[f]	−0.43[e]
	416 (35.2)	2.98		

[a] Data taken from Ref. [10].
[b] Solutions *ca.* 3–8 × 10^{-5} M.
[c] Measured in solutions *ca.* 10^{-3} M in analyte and 0.1 M in $[NBu^n_4]PF_6$ at a 2 mm disc glassy carbon working electrode with a scan rate of 200 mV s^{-1}. Ferrocene internal reference $E_{1/2}$ = 0.44 V, ΔE_p = 90 mV.
[d] Irreversible, $i_{pa} > i_{pc}$.
[e] E_{pc} for an irreversible reduction process.
[f] E_{pa} for an irreversible oxidation process.

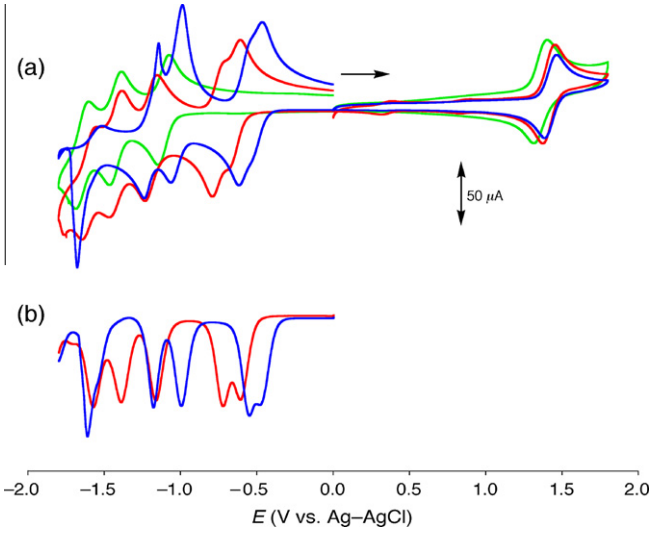

Fig. 5. (a) Cyclic voltammograms for the complex salts **1** (green), **2** (red) and **3** (blue) recorded at 200 mV s^{-1} in acetonitrile with a glassy carbon working electrode. The arrow indicates the direction of the initial scans. (b) Differential pulse voltammograms for the complex salts **2** (red) and **3** (blue) recorded under the same conditions (potential increment = 4 mV; amplitude = 50 mV; pulse width = 0.01 s) (Colour online).

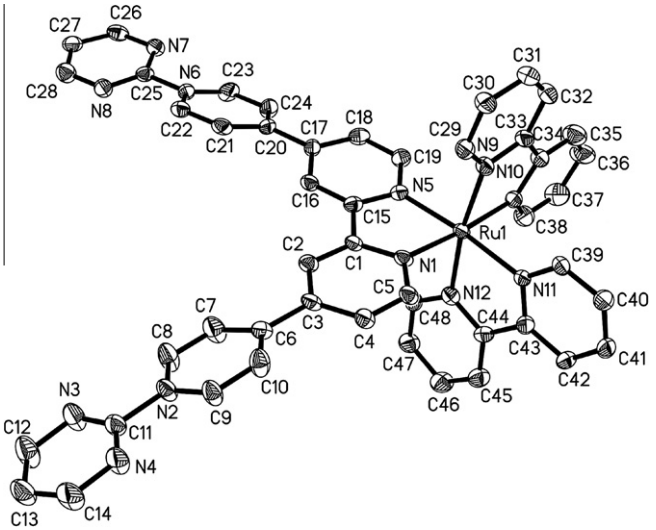

Fig. 7. Representation of the molecular structure of the complex cation in the salt **5**·2.75MeCN, with the H atoms removed for clarity (30% probability ellipsoids).

pyridinium substituents both red shifts and enhances the intensities of the MLCT absorptions.

For the qpy-based complexes, the energies of both MLCT bands decrease slightly on moving from R = Me to Ph (**2** → **3**), but the differences between the E_{max} values for the complexes with R = Ph, 4-AcPh, 3,5-MC_2Ph or 4-MCPh are minimal. Similar behaviour is also observed for the tris-chelates, $[Ru^{II}(R_2qpy^{2+})_3]^{8+}$ (R = Me, Ph, 4-AcPh or 3,5-MC_2Ph) [10]. The complexes with the most strongly electron-withdrawing substituents, 2-Pym and 2,4-DNPh, logically exhibit the most red-shifted MLCT bands. However, the total shifts in E_{max} are relatively small; on moving from **2** to **5**, −0.06 eV for the LE band and −0.08 eV for the HE band (Fig. 3). The same general

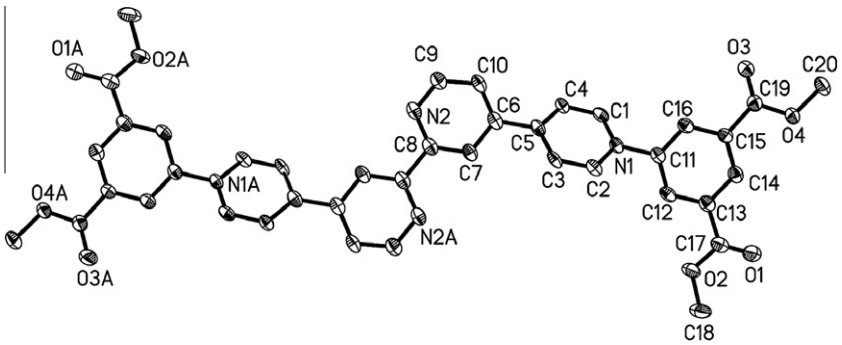

Fig. 6. Representation of the molecular structure of the cation in the salt $[(3,5\text{-}MC_2Ph)_2qpy^{2+}]Cl_2{\cdot}5CD_3OD$, with the H atoms removed for clarity (50% probability ellipsoids).

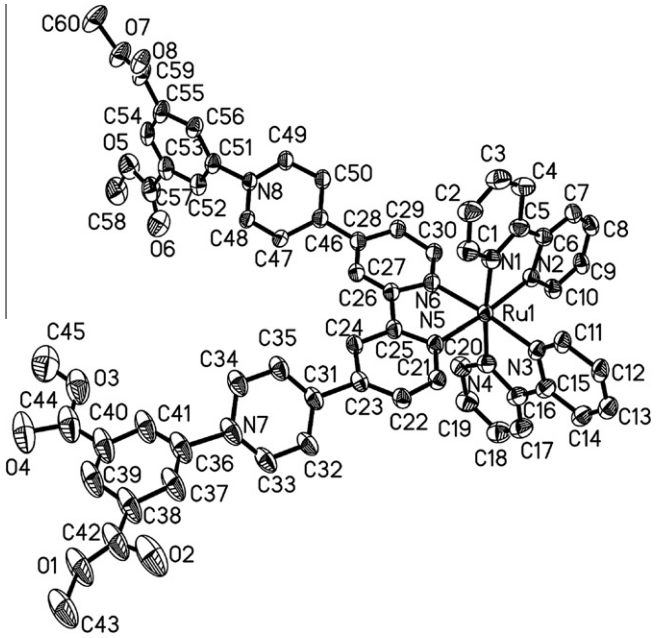

Fig. 8. Representation of the molecular structure of the complex cation in the salt **7**·2.5MeCN, with the H atoms removed for clarity (30% probability ellipsoids).

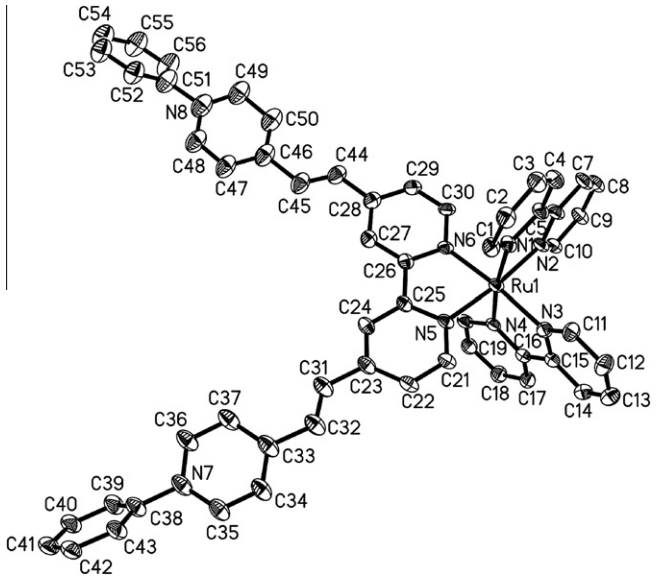

Fig. 9. Representation of the molecular structure of the complex cation in the salt **10**·2MeCN, with the H atoms removed for clarity (30% probability ellipsoids).

trend is also observed for the complexes $[Ru^{II}(NH_3)_4(R_2qpy^{2+})]^{4+}$ (R = Me, Ph, 4-AcPh or 2-Pym) [9], although these ammine chromophores show only one visible maximum that shifts to a much greater extent; −0.25 eV on replacing Me with 2-Pym.

For the new bbpe-based series, the energies of both MLCT bands decrease slightly on moving from **9** to **11** (Fig. 4), with differences of 0.05 and 0.06 eV between the extreme E_{max} values. The HE MLCT band red shifts by 0.07–0.08 eV on moving from a qpy-based complex to its bbpe analogue, but the LE MLCT band shows very slight accompanying blue shifts of 0.01–0.02 eV. These observations are consistent with stabilisation of the acceptor MO by increased delocalisation when this orbital is located primarily on the outer parts of the quaternised ligands (for the HE transition), but destabilisation of the acceptor MO due to the mild electron-donating influence of ethenylene units when this orbital is located primarily on the bpy groups (for the LE transition).

Table 4
Selected interatomic distances (Å) and angles (°) for the complex salts **5**·2.75MeCN, **7**·2.5MeCN and **10**·2MeCN.

	5·2.75MeCN	**7**·2.5MeCN	**10**·2MeCN
Ru–N(L^A)	2.044(7)	2.035(17)	2.046(12)
Ru–N(L^A)	2.047(7)	2.053(17)	2.034(12)
Ru–N(bpy, trans-L^A)	2.064(7)	2.038(17)	2.043(12)
Ru–N(bpy, trans-L^A)	2.067(7)	2.036(18)	2.061(12)
Ru–N(bpy, trans-bpy)	2.051(8)	2.065(18)	2.056(12)
Ru–N(bpy, trans-bpy)	2.077(7)	2.078(18)	2.077(12)
N(L^A)–Ru–N(L^A)	78.9(3)	78.7(7)	79.5(5)
N(bpy)–Ru–N(bpy)	79.0(3)	79.3(7)	79.2(5)
N(bpy)–Ru–N(bpy)	78.4(3)	79.6(8)	79.6(5)
Dihedral angles 1[a]	21.0, 21.0	26.3, 39.0	6.1, 4.0/17.5, 18.6[c]
Dihedral angles 2[b]	5.9, 20.0	64.9, 45.9	54.4, 45.9/46.5, 35.8[c]

L^A = $(2\text{-Pym})_2qpy^{2+}$ (in **5**), $(3,5\text{-MC}_2\text{Ph})_2qpy^{2+}$ (in **7**) or Ph_2bbpe^{2+} (in **10**).
[a] Between the planes of the two pyridyl rings within the two halves of the L^A ligands.
[b] Between the planes of the quaternised pyridyl and *N*-aryl substituent within the two halves of the L^A ligands.
[c] For the two independent cations in the asymmetric unit.

The new UV–Vis data also merit quantitative comparisons with those obtained previously for the complexes $[Ru^{II}(R_2qpy^{2+})_3]^{8+}$ (Table 3). When compared with these tris-chelates, the MLCT bands of the *cis*-$[Ru^{II}(bpy)_2(R_2qpy^{2+})]^{4+}$ complexes are always red shifted but less intense. On moving from a mono-R_2qpy^{2+} complex to its tris-R_2qpy^{2+} counterpart, the E_{max} value of the LE MLCT band increases by 0.04–0.07 eV, while that of the HE MLCT band increases by 0.13–0.25 eV. These energy changes become smaller on moving along the series R = Me > Ph > 4-AcPh ≈ $3,5MC_2Ph$. The observation of larger relative changes for the HE band is consistent with the assignment of this absorption as being more strongly associated with the presence of pyridinium substituents (see above). Given that the ligand structure remains constant, the blue shifts in the MLCT bands on increasing the number of pyridinium groups imply stabilisation of the Ru-based HOMO (see below).

3.4. Electrochemical studies

The complex salts **1**–**13** were studied by cyclic voltammetry in acetonitrile and the results are presented in Table 2. When using a glassy carbon working electrode, all of the complexes show quasi-reversible or reversible $Ru^{III/II}$ oxidation waves, together with two or more ligand-based reduction processes that range in character from reversible to irreversible. $E_{1/2}$ values are reported for the latter waves only in cases where the i_{pa} and i_{pc} values are equivalent, while E_{pa} and E_{pc} values are quoted otherwise.

The $[E_{1/2}]Ru^{III/II}$ value increases by 50–80 mV on moving from **1** to its quaternised derivatives (Table 2, Fig. 5), indicating stabilisation of the Ru-based HOMO due to the electron-withdrawing influence of the pyridinium groups. Clearly, significant electronic coupling occurs between the Ru^{II} centre and pyridinium moieties. The differences in $[E_{1/2}]Ru^{III/II}$ between **2** and the *N*-aryl derivatives are small but consistent at *ca.* 20–30 mV. For the series **9**–**11**, the mildly electron-donating influence of the ethenylene units offsets the withdrawing effect of the quaternised groups, giving $[E_{1/2}]Ru^{III/II}$ values indistinguishable from that of **1**.

The potentials for ligand-based reduction increase on moving from **1** to its quaternised derivatives (Fig. 5), indicating stabilisation of the LUMOs. These energy changes are more pronounced than those for the HOMO, consistent with the observed red-shifts in the MLCT bands (see above). Moving along the series **2** to **5**, the potential of the first reduction process increases by a total of *ca.* 400 mV, and the overall trend observed with respect to the

increasing electron-withdrawing strength of the pyridinium moieties is reminiscent of that found in other Ru^{II} complexes of monodentate 4,4′-bipyridinium ligands [9,22,23]. The first reduction process for complex salts **2** and **3** is actually two strongly overlapped waves which can be resolved by using differential pulse voltammetry (Fig. 5). This behaviour shows that the initial reduction of one of the pyridinium groups affects the potential for the other one, due to significant electronic coupling within the coordinated qpy unit. Similar effects are observed for the related species $[Ru^{II}(NH_3)_4(R_2qpy^{2+})][PF_6]_4$ (R = Me or Ph) [9], although the potentials for the latter are cathodically shifted by 60–120 mV when compared with those of **2** and **3**. These differences are due to the higher electron-donating ability of the ammine ligands with respect to bpy that is transmitted to the R_2qpy^{2+} ligands *via* the Ru^{II} centre. The presence of the ethenylene groups causes the reductive chemistry of **9**–**11** to be completely irreversible because the radical anions generated are prone to undergo rapid chemical reactions.

The $Ru^{III/II}$ waves for **2**–**4** and **7** are found at lower potentials by *ca.* 200 mV when compared with the analogous $[Ru^{II}(R_2qpy^{2+})_3]^{8+}$ complexes (Tables 2 and 3). This difference is attributable to the presence of only two as opposed to six pyridinium substituents that renders the Ru centres more electron rich in the new complexes. Hence, the blue shifts in the MLCT bands on increasing the number of pyridinium groups are indeed due to stabilisation of the Ru-based HOMO (see above). In contrast, the first ligand-based reductions occur at generally similar potentials in **2**–**4** and **7** when compared with their $[Ru^{II}(R_2qpy^{2+})_3]^{8+}$ analogues, indicating that electronic coupling between the three bpy-based ligands is weak.

3.5. Crystallographic studies

Single-crystal X-ray structures have been obtained for the complex salts **5**·2.75MeCN, **7**·2.5MeCN and **10**·2MeCN, and also for the pro-ligand salt $[(3,5\text{-}MC_2Ph)_2qpy^{2+}]Cl_2\cdot 5CD_3OD$. Representations of the molecular structures are shown in Figs. 6–9, and selected interatomic distances and angles for the complex salts are presented in Table 4.

The structure of $[(3,5\text{-}MC_2Ph)_2qpy^{2+}]Cl_2\cdot 5CD_3OD$ resembles that we have determined previously for the related compound $[Ph_2qpy^{2+}][PF_6]_2\cdot Me_2CO$ [9], with a planar, transoid bpy unit with a crystallographic centre of symmetry in the middle of the C–C bond between the pyridyl rings. As for Ph_2qpy^{2+}, the rest of the $(3,5\text{-}MC_2Ph)_2qpy^{2+}$ molecule is strongly twisted, with dihedral angles of 32.9° within the 4,4-bipyridyl fragments and 41.4° between the pyridyl and attached phenyl rings. All other geometric parameters for these two qpy-based dications are very similar.

Although the uncertainties on the data for **5**·2.75MeCN, **7**·2.5MeCN and **10**·2MeCN are quite large, the average Ru–N distance to the L^A ligands (*ca.* 2.04 Å) does seem to be a little smaller than the Ru–N(bpy) distances (average *ca.* 2.06 Å); if truly significant then this observation is consistent with a slight increase in π-back-bonding to the more strongly electron-withdrawing L^A ligands. These ligands adopt fairly twisted conformations, with the dihedral angles between the pyridyl rings being generally smaller than those between the pyridyl and attached aryl rings, except for the $(2\text{-}Pym)_2qpy^{2+}$ in **5**·2.75MeCN (Table 4). Other structures of *N*-(2-Pym)pyridyl derivatives have also revealed relatively small twists within these moieties [23,24]. To our knowledge, the only other reported structure containing a Ru^{II}(qpy) motif is a metallomacrocycle with two *cis*-$[Ru^{II}(bpy)_2qpy]^{2+}$ units and two *fac*-{$Re^{I}Cl(CO)_3$} moieties [25]. While the level of precision of that structure is similar to those for our new ones, average relative shortenings of the Ru–N(qpy) with respect to the Ru–N(bpy) distances of *ca.* 0.02–0.03 Å are again observed. Incidentally, because all three of the new complex salts adopt centrosymmetric crystal packing structures, they are not expected to show significant bulk second-order NLO effects.

4. Conclusion

A large series of new complexes of the form *cis*-$[Ru^{II}(bpy)_2(L^A)]^{4+}$ (L^A = a pyridinium-substituted bpy derivative) has been prepared and fully characterised. These asymmetric species are intermediates between the archetypal MLCT chromophore RuTB and recently reported extended tris-chelates $[Ru^{II}(L^A)_3]^{8+}$ that show marked NLO properties. The UV–Vis spectra of the new complex salts feature intense intraligand $\pi \rightarrow \pi^*$ absorptions and also MLCT bands with two distinct visible maxima. Small shifts in these bands correlate with the relative electron-withdrawing strength of L^A. Cyclic voltammograms show quasi-reversible or reversible $Ru^{III/II}$ oxidation waves, together with two or more ligand-based reduction processes that range in character from reversible to irreversible. The variations in the redox potentials correlate with changes in the structure of L^A, and also with the MLCT energies. Differential pulse voltammetry allows the first reduction process for complex salts **2** and **3** to be resolved into two peaks. Single-crystal X-ray structures have been solved for a pro-ligand salt and for three of the new complex salts, affording rare examples of crystallographically-characterised Ru^{II}(qpy) motifs. The carboxylate-functionalised compounds **12** and **13** have been tested as photosensitizers on TiO_2-coated electrodes, but show only negligible efficiencies, so further details will not be discussed here. However, these observations are consistent with previous reports in that RuTB derivatives do not make especially good sensitizers [26]; this field is dominated by Ru^{II} bis-bpy complexes with thiocyanate coligands [6]. In addition to containing RuTB cores, **12** and **13** have relatively long bridges between the Ru^{II} centre and carboxylate groups. This factor together with interannular twisting within these bridges can be expected to hinder electron injection into a semiconductor surface.

Acknowledgement

We thank the EPSRC for support in the form of PhD studentships (ECH and YTT), and Dr Hongxia Wang (Bath University) for carrying out TiO_2 photosensitization studies with **12** and **13**.

Appendix A. Supplementary data

CCDC 810529, 810530, 810531 and 810532 contains the supplementary crystallographic data for ($[(3,5\text{-}MC_2Ph)_2qpy^{2+}]Cl_2\cdot 5CD_3OD$), (**5**·2.75MeCN), (**7**·2.5MeCN) and (**10**·2MeCN). These data can be obtained free of charge via http://www.ccdc.cam.ac.uk/conts/retrieving.html, or from the Cambridge Crystallographic Data Centre, 12 Union Road, Cambridge CB2 1EZ, UK; fax: (+44) 1223-336-033; or e-mail: deposit@ccdc.cam.ac.uk.

References

[1] (a) M.A. Bennett, M.I. Bruce, T.W. Matheson, in: G. Wilkinson, F.G.A. Stone, E.W. Abel (Eds.), Comprehensive Organometallic Chemistry, vol. 4, Pergamon Press, Oxford, 1982, pp. 651–965;
(b) M. Schröder, T.A. Stephenson, in: G. Wilkinson, R.D. Gillard, J.A. McCleverty (Eds.), Comprehensive Coordination Chemistry, vol. 4, Pergamon Press, Oxford, 1987, pp. 277–518;
(c) M.A. Bennett, M.I. Bruce, M.P. Cifuentes, A.J. Deeming, R.J. Haines, A.F. Hill, M.G. Humphrey, K. Khan, R.K. Pomeroy, E. Sappa, A.K. Smith, E. Wenger, in: E.W. Abel, F.G.A. Stone, G. Wilkinson (Eds.), Comprehensive Organometallic Chemistry II, vol. 7, Pergamon Press, Oxford, 1995, pp. 291–960;
(d) C.-M. Che, C.E. Housecroft, T.-C. Lau, in: J.A. McCleverty, T.J. Meyer (Eds.), Comprehensive Coordination Chemistry II, vol. 5, Pergamon Press, Oxford, 2004, pp. 555–847;
(e) I.R. Butler, V. Cadierno, M.P. Cifuentes, P. Crochet, P.J. Dyson, J. Gimeno, M.G. Humphrey, A.L. Johnson, B.K.L. Leong, J.S. McIndoe, R.K. Pomeroy, P.R.

Raithby, E. Sappa, H. Suzuki, T. Takao, D. Thomas, M.K. Whittlesey, J.D. Wilton-Ely, W.-T. Wong, in: R.H. Crabtree, D.M.P. Mingos (Eds.), Comprehensive Organometallic Chemistry III, vol. 6, Pergamon Press, Oxford, 2007, pp. 353–1116.
[2] (a) Selected recent reviews: C. Samojłowicz, M. Bieniek, K. Grela, Chem. Rev. 109 (2009) 3708;
(b) J.J. Concepcion, J.W. Jurss, M.K. Brennaman, P.G. Hoertz, A.O.T. Patrocinio, N.Y. Murakami Iha, J.L. Templeton, T.J. Meyer, Acc. Chem. Res. 42 (2009) 1954;
(c) S.P. Nolan, H. Clavier, Chem. Soc. Rev. 39 (2010) 3305;
(d) W.P. Griffith, Ruthenium Oxidation Complexes: Their Uses as Homogenous Organic Catalysts (Catalysis by Metal Complexes), Springer, Dordrecht, 2010.
[3] (a) Selected reviews: M.J. Clarke, Coord. Chem. Rev. 236 (2003) 209;
(b) I. Kostova, Curr. Med. Chem. 13 (2006) 1085;
(c) W.H. Ang, P.J. Dyson, Eur. J. Inorg. Chem. (2006) 4003;
(d) P.C.A. Bruijnincx, P.J. Sadler, Adv. Inorg. Chem. 61 (2009) 1.
[4] (a) Selected reviews: A. Juris, V. Balzani, F. Barigelletti, S. Campagna, P. Belser, A. von Zelewsky, Coord. Chem. Rev. 84 (1988) 85;
(b) V. Balzani, A. Juris, Coord. Chem. Rev. 211 (2001) 97;
(c) J.G. Vos, J.M. Kelly, Dalton Trans. (2006) 4869;
(d) S. Campagna, F. Puntoriero, F. Nastasi, G. Bergamini, V. Balzani, Top. Curr. Chem. 280 (2007) 117;
(e) L. Herman, S. Ghosh, E. Defrancq, A. Kirsch-De Mesmaeker, J. Phys. Org. Chem. 21 (2008) 670;
(f) S. Bonnet, J.-P. Collin, Chem. Soc. Rev. 37 (2008) 1207.
[5] (a) Selected examples: M. Buda, G. Kalyuzhny, A.J. Bard, J. Am. Chem. Soc. 124 (2002) 6090;
(b) S. Welter, K. Brunner, J.W. Hofstraat, L. De Cola, Nature 421 (2003) 54;
(c) Y.-L. Tung, L.-S. Chen, Y. Chi, P.-T. Chou, Y.-M. Cheng, E.Y. Li, G.-H. Lee, C.-F. Shu, F.-I. Wu, A.J. Carty, Adv. Funct. Mater. 16 (2006) 1615;
(d) J.D. Slinker, J. Rivnay, J.S. Moskowitz, J.B. Parker, S. Bernhard, H.D. Abruña, G.G. Malliaras, J. Mater. Chem. 17 (2007) 2976.
[6] (a) M.K. Nazeeruddin, M. Grätzel, in: J.A. McCleverty, T.J. Meyer (Eds.), Comprehensive Coordination Chemistry II, vol. 9, Pergamon Press, Oxford, UK, 2004, pp. 719–758;
(b) N. Robertson, Angew. Chem., Int. Ed. 45 (2006) 2338;
(c) J.R. Durrant, S.A. Haque, E. Palomares, Chem. Commun. (2006) 3279;
(d) S. Ardo, G.J. Meyer, Chem. Soc. Rev. 38 (2009) 115;
(e) A. Hagfeldt, G. Boschloo, L.-C. Sun, L. Kloo, H. Pettersson, Chem. Rev. 110 (2010) 6595.
[7] (a) Selected examples: F.H. Burstall, J. Chem. Soc. (1936) 173;
(b) D.P. Rillema, D.S. Jones, H.A. Levy, J. Chem. Soc., Chem. Commun. (1979) 849;
(c) A. Juris, V. Balzani, P. Belser, A. von Zelewsky, Helv. Chim. Acta 64 (1981) 2175.
[8] B.J. Coe, in: M.G. Papadopoulos, J. Leszczynski, A.J. Sadlej (Eds.), Nonlinear Optical Properties of Matter: From Molecules to Condensed Phases, Springer, Dordrecht, 2006, pp. 571–608.
[9] B.J. Coe, J.A. Harris, L.A. Jones, B.S. Brunschwig, K. Song, K. Clays, J. Garín, J. Orduna, S.J. Coles, M.B. Hursthouse, J. Am. Chem. Soc. 127 (2005) 4845.
[10] B.J. Coe, J.A. Harris, B.S. Brunschwig, I. Asselberghs, K. Clays, J. Garín, J. Orduna, J. Am. Chem. Soc. 127 (2005) 13399.
[11] B.J. Coe, M. Samoc, A. Samoc, L.-Y. Zhu, Y.-P. Yi, Z.-G. Shuai, J. Phys. Chem. A 111 (2007) 472.
[12] B.P. Sullivan, D.J. Salmon, T.J. Meyer, Inorg. Chem. 17 (1978) 3334.
[13] B.J. Coe, J. Fielden, S.P. Foxon, B.S. Brunschwig, I. Asselberghs, K. Clays, A. Samoc, M. Samoc, J. Am. Chem. Soc. 132 (2010) 3496.
[14] SAINT (Version 6.45), Bruker AXS Inc., Madison, Wisconsin, USA, 2003.
[15] SADABS (Version 2.10), Bruker AXS Inc., Madison, Wisconsin, USA, 2003.
[16] G.M. Sheldrick, Acta Crystallogr., Sect. A 46 (1990) 467.
[17] G.M. Sheldrick, SHELXS 97, Programs for Crystal Structure Analysis (Release 97–2), University of Göttingen, Göttingen, Germany, 1997.
[18] SHELXTL (Version 6.10), Bruker AXS Inc., Madison, Wisconsin, USA, 2000.
[19] (a) See for examples: K. Bierig, R.J. Morgan, S. Tysoe, H.D. Gafney, T.C. Strekas, A.D. Baker, Inorg. Chem. 30 (1991) 4898;
(b) M.A. Hayes, C. Meckel, E. Schatz, M.D. Ward, J. Chem. Soc., Dalton Trans. (1992) 703;
(c) R.J. Forster, T.E. Keyes, J. Phys. Chem. B 102 (1998) 10004.
[20] A. Shi, M.R. Pokhrel, S.H. Bossmann, Synthesis 4 (2007) 505.
[21] R.J. Morgan, A.D. Baker, J. Org. Chem. 55 (1990) 1986.
[22] (a) B.J. Coe, J.A. Harris, L.J. Harrington, J.C. Jeffery, L.H. Rees, S. Houbrechts, A. Persoons, Inorg. Chem. 37 (1998) 3391;
(b) B.J. Coe, J.A. Harris, I. Asselberghs, A. Persoons, J.C. Jeffery, L.H. Rees, T. Gelbrich, M.B. Hursthouse, J. Chem. Soc., Dalton Trans. (1999) 3617.
[23] B.J. Coe, T. Beyer, J.C. Jeffery, S.J. Coles, T. Gelbrich, M.B. Hursthouse, M.E. Light, J. Chem. Soc., Dalton Trans. (2000) 797.
[24] (a) B.J. Coe, J.A. Harris, I. Asselberghs, K. Wostyn, K. Clays, A. Persoons, B.S. Brunschwig, S.J. Coles, T. Gelbrich, M.E. Light, M.B. Hursthouse, K. Nakatani, Adv. Funct. Mater. 13 (2003) 347;
(b) B.J. Coe, S.P. Foxon, E.C. Harper, J.A. Harris, M. Helliwell, J. Raftery, I. Asselberghs, K. Clays, E. Franz, B.S. Brunschwig, A.G. Fitch, Dyes Pigments 81 (2009) 171;
(c) B.J. Coe, R.J. Docherty, S.P. Foxon, E.C. Harper, M. Helliwell, J. Raftery, K. Clays, E. Franz, B.S. Brunschwig, Organometallics 28 (2009) 6880.
[25] P. de Wolf, P. Waywell, M. Hanson, S.L. Heath, A.J.H.M. Meijer, S.J. Teat, J.A. Thomas, Chem. Eur. J. 12 (2006) 2188.
[26] (a) K. Kalyanasundaram, Md.K. Nazeeruddin, M. Grätzel, G. Viscardi, P. Savarino, E. Barni, Inorg. Chim. Acta 198-200 (1992) 831;
(b) V. Aranyos, J. Hjelm, A. Hagfeldt, H. Grennberg, Dalton Trans. (2003) 1280.